MUONIUM PRODUCTION FROM FINE SILICA POWDER

by

Anna Cornelia Janissen

A THESIS SUBMITTED IN PARTIAL FULFILLMENT
OF THE REQUIREMENTS FOR THE DEGREE OF
MASTER OF SCIENCE
in the Department
of Physics

We accept this thesis as conforming
to the required standard

[redacted]

Supervisor: Dr. A. Olin

[redacted]

Supervisor: Dr. G.A. Beer

[redacted]

Dr. G.R. Mason

[redacted]

Dr. D. Harrington

[redacted]

Dr. P. Romaniuk

UNIVERSITY OF VICTORIA

Abstract

Joint Supervisors: Dr. G.A. Beer and Dr. A. Olin.

The muonium atom, μ^+e^- , is an ideal system from which to gain information about the $e-\mu$ interaction both to test the existing theory of QED and to search for physics beyond the standard model. A systematic study has been carried out of the production and properties of thermal muonium from a fine silica powder, Cab-O-Sil. Properties such as the angular distribution are examined, as well as the experimental conditions resulting in the optimum production rate. The particular features of Cab-O-Sil which give it its muonium producing capability are investigated by considering other forms of silica. All of these investigations are carried out in the context of a Fick's Law diffusion model the validity of which is examined finally.

Examiners:

[redacted]

Dr. A. Olin

[redacted]

Dr. G.A. Beer

[redacted]

Dr. G.R. Mason

[redacted]

Dr. D. Harrington

[redacted]

Dr. P. Romaniuk

Contents

List of Figures

List of Tables

Acknowledgements

I would like to acknowledge the efforts of the MUBAR group who collected the data for this work in connection with the muonium conversion experiment, including G. Beer, T. Bowen, A. Fry, Z. Gelbart, P. Halverson, T. Huber, K. Kendall, R. Kunselman, G. Marshall, G. Mason, A. Olin, and J. Warren.

I would like to especially thank my co-supervisor Art Olin, with whom the analysis was carried out, for his help and encouragement, and for his invaluable advice on the writing of this thesis.

Finally, many thanks go to D. Britton who patiently listened to all of the tribulations associated with this work.

For my family.

Chapter 1

Motivation

The atom muonium, μ^+e^- or Mu, is formed in the final stage of the process whereby a positive muon loses its energy through interactions with matter. Being the simplest bound state of an electron and a muon, muonium is the ideal system from which to gain information about the e - μ interaction.[1] In particular, measurement of the hyperfine structure [2] and Zeeman energy levels [3] provide sensitive tests of quantum electrodynamics, QED. The most precise value for the magnetic moment and the mass of the muon are derived from the Zeeman effect measurement in the muonium ground state. Measurement of the muonium Lamb shift [4,5] provides another test of QED. In fact, this measurement is potentially a cleaner test than the Lamb shift in hydrogen, because of the absence of corrections due to proton structure. The μ^+e^- system is also a convenient place to look for the effects of new interactions such as the lepton number violating process of muonium conversion to antimuonium, μ^-e^+ or $\overline{\mathrm{Mu}}$ [6,7]. The technique for producing muonium described in this work was developed for this conversion measurement.

Formation of muonium was first observed by Hughes et al. [8] Polarized muons were stopped in a target of argon gas at 50 atm. pressure. Identification was made by observing the characteristic Larmor precession frequency of muonium. Although this technique produced a large yield of muonium, (85 $\pm$ 9) % of the incoming muons in low pressure Ar [9], it was recognized

that the usefulness of muonium would increase if it could be produced in a vacuum. For example, muonium and antimuonium have degenerate energy levels in zero magnetic field. The rate of conversion of Mu to $\overline{\mathrm{Mu}}$ falls off by a factor of more than 2 in fields of > 10 mG. And so the optimal conditions for observation of this conversion include muonium in a field free region. This implies no collisions with moderator atoms such as Ar. Similarly, the measurement of the muonium Lamb shift in the n=2 state must be carried out in a vacuum since collisions with other atoms quench the Mu(2s) signal. A recent measurement of the 1s-2s laser induced transition was also done in vacuum [10].

In order to produce muonium in vacuum, the beam-foil method was developed [11,12] in which a low energy muon beam is passed through a thin foil of metal, typically gold or aluminum. Muonium atoms emerge from the foils with energies of less than 20 keV. In order to separate the small neutral component from the rest of the beam a sweeping magnetic field is applied. Of course this field would be inconvenient for a muonium conversion experiment where muonium in a field-free region is preferable. Another problem with the beam-foil technique is a relatively low muonium yield of approximately 0.03 % of the incoming muons. By comparison, Cab-O-Sil, a powder of SiO_2 , produces a yield per incident muon of ~ 2 %. In addition to having a low yield, the muonium which is produced by this technique is moving with epithermal velocities typically 0.01 times the speed of light. This means that in a muon lifetime the muonium atom would travel 6 m.

Production of muonium with thermal velocities was attempted by Kendall et al [13]. who studied muonium diffusing out of hot tungsten and platinum foils. Positive results were obtained but duplicating them proved difficult. Mills et al. [14] studied hot W foils and report having seen a muonium yield of (4 ± 2)% of the stopped muons. These results too have been difficult to

duplicate since the technique is sensitive to the cleanliness of the W surface. In addition, the technique requires heating a foil to 2800 K which produces a high magnetic field and so limits the utility of the muonium produced.

Most recently [15], a fine powder of SiO_2 , known as Cab-O-Sil, has been used. It is powder composed of small spheres, 3.5 to 7 nm radius, of amorphous SiO_2 . These spheres come together in the formation process to form long chain-like aggregates with large spaces in between. The muonium produced from Cab-O-Sil travels with thermal velocities which means that in a muon lifetime the atoms will travel only $\sim$ 2 cm. This enables experiments, such as the search for muonium conversion or the 1s-2s transition energy measurement, to examine the entire Mu cloud instead of having to sample it.

What follows is a systematic study of the production and properties of thermal muonium from Cab-O-Sil. The Mu yield is first measured with the aid of a computer simulation. Then effects such as the angular distribution of the muonium, the dependence of the yield on the gas pressure in the vacuum system and the muon stopping distribution in the powder layer are examined. The particular features, such as low density and high surface area, which give Cab-O-Sil its Mu producing capability are investigated by examining other forms of SiO_2 . All of these investigations are carried out in the context of a Fick's Law diffusion model the validity of which is examined finally.

Chapter 2

Formation of Muonium in Cab-O-Sil

Cab-O-Sil [16], is fine powder of amorphous silicon dioxide. It is formed by burning silicon tetrachloride vapor in a flame of hydrogen and oxygen. In the burning process, molten SiO_2 spheres of diameters between 7 and 14 nm are formed. While cooling, these spheres collide with each other and fuse together into three dimensional chain-like aggregates which exhibit a self-similar, or fractal, structure [17,18]. The resulting powder has a surface area of between 400 m^2/g and 200 m^2/g depending on the grade. For this experiment the finest grade available, 7 nm diameter spheres, was used. The rationale behind using this powder is that the powder grains are very small and so once the muonium atoms are formed inside the SiO_2 grains, they can relatively quickly diffuse to the surface, evaporate off of the grains and move into the spaces between the chains. The muonium can then, in a random walk, move in between the chain-like aggregates out of the powder layer and into the vacuum.

The formation of muonium in Cab-O-Sil is a three stage process. First, the μ^+ stops in the SiO_2 grains. The fraction of muons which form muonium inside the grains themselves is the same as the fraction in bulk quartz. This fraction has been measured [19], using a μSR technique, as 0.61 ± 0.03.

The muonium must then diffuse to the surface of an individual grain and evaporate into the vacuum spaces between grains. The fraction that do so has been estimated using a diffusion model. This model assumes that there exists

some barrier, such as a work function, which prevents a muonium atom from re-entering a grain once it has left. It has been found that for grains of 7 nm diameter (97 $\pm$ 1) % of the muonium atoms emerge from individual grains into the vacuum spaces between grains [20,21].

The atoms must next diffuse to the surface of the layer itself in order to get out of the powder and into the vacuum. Fick's Law states that

$$\mathbf{\Gamma} = -D\ \nabla W(\mathbf{r}, t). \tag{2.1}$$

where Γ is the flow of diffusing atoms through a layer of uniformly distributed grains of SiO_2 , W is the probability per unit area of finding the Mu atom at a position $\mathbf{r}$ and at time t, and D is the proportionality constant of the diffusion process. Validity of Fick's Law is a fundamental assumption of the model since the diffusion could, in fact, have a different nature. For example, it is known that the chain-like aggregates of Cab-O-Sil have a fractal structure. Diffusion of particles along a fractal lattice, as opposed to a Euclidean one, does not obey Fick's law but rather a generalization of it incorporating the notion that the diffusion takes place in a non-integer dimension [22]. Within the framework of regular diffusion, however, Fick's law leads to the diffusion equation:

$$\frac{dW}{dt} = D\ \nabla^2 W. \tag{2.2}$$

with D being the proportionality factor defined above and is called the diffusion constant. To model the diffusion out of a powder layer a boundary condition can be applied to this equation which is that $W = 0$ on the surface of the powder layer. This surface acts as a perfect absorbing interface, which means physically that once a Mu atom has left the layer it does not return. The general solution of equation (2.2) is:

$$W(\mathbf{r}, t)\, d\mathbf{r} = \frac{1}{(4\pi Dt)^{\frac{3}{2}}}\ \exp\left[-\frac{|\mathbf{r}|^2}{4Dt}\right]\ d\mathbf{r}. \tag{2.3}$$

The probability that a particle, decaying at a rate of λ per second, has crossed a layer of thickness d is then:

$$P = -\int_0^\infty dt\, e^{-\lambda t}\, D[\hat{\mathbf{n}} \cdot \nabla W(\mathbf{r},t)]|_{W=0\,at\,d}. \tag{2.4}$$

It is important to note what geometrical assumptions are inherent in the above probability. This expression assumes an infinite powder layer size in two dimensions However, the boundary condition on W will incorporate a finite layer thickness, d, in the third dimension.

Once the diffusion constant is known, the above expression can be used to calculate the yield of Mu which will emerge from the powder. Two ways of calculating this diffusion constant have been attempted. The first method is analytical estimation and was attempted by Marshall. [21] The diffusion constant D can also be written as:

$$D = \frac{cs}{3} \tag{2.5}$$

where c is the mean speed and s is the mean free path of a point particle, in this case the muonium atom. Now assuming that the material through which the muonium is diffusing is a uniform, random collection of n per cm^3 stationary spheres of radius r, the mean free path is:

$$s = \frac{1}{\pi r^2 n}. \tag{2.6}$$

The number density of silica powder grains n is related to the density of bulk silica, ρ, and the density of Cab-O-Sil, ρ', by:

$$n = \frac{3\rho'}{4\pi r^3 \rho}. \tag{2.7}$$

Then the diffusion constant can be calculated by:

$$D = \frac{4}{9} cr \left(\frac{\rho}{\rho'}\right). \tag{2.8}$$

At room temperature, using a Boltzmann velocity distribution, the mean thermal velocity of muonium is 7.37×10^5 cm/s. The density of bulk silica is $\rho = 2.64$ g/cm^3, and the density of Cab-O-Sil is $\rho' = 0.032$ g/cm^3. The grade of Cab-O-Sil used was EH5 which has a grain radius of $r = 3.5$ nm. Then using (2.8) the diffusion constant is:

$$D = 9.5 \text{ cm}^2/\text{s}.$$

The second method of obtaining the diffusion constant is the one employed in this work. A critical assumption in the above calculation of the mean free path is that the Cab-O-Sil is a uniform random collection of spheres. It is known from electron micrographs of the powder, however, that this is not the case. The tendency of the spheres to form chains with long spaces in between would tend to increase the mean free path of a diffusing Mu atom and so increase the effective diffusion constant. For this reason a Monte Carlo computer simulation was employed in which the diffusion constant was treated as a free parameter to be fit to the data. As will be discussed in the final chapter, an effective diffusion constant for diffusion of Mu through Cab-O-Sil was found to be 620 ± 80 cm^2/s. Using equation (2.5) this diffusion constant implies a mean free path roughly two orders of magnitude larger than the above analytical approximation.

Chapter 3

Apparatus

The apparatus used for muonium yield measurements is very similar to a system described elsewhere [23]. The present apparatus is shown in figure 3.1. The TRIUMF surface muon channel, M15, delivered low-energy positive muons at a rate of 6×10^4/s. The rate was limited by slits in order to allow only 1 μ^+ in the apparatus at a time. The beam was of nominal central momentum 28.5 ± 0.3 MeV/c, and either 3 or 10% (FWHM) momentum spread depending on the aspect of the experiment being investigated. The beam initially passed through a thin aluminized mylar mirror designed to collect light from a beam counter, which was a 3.8 cm diameter, 0.25 mm thick plastic scintillator. The beam next passed through a 0.025 mm stainless steel vacuum window which separated the beamline vacuum from the ultra-high vacuum system used. This vacuum system was designed for an experiment to search for the conversion of Mu to $\overline{\mathrm{Mu}}$, called the MUBAR experiment, for which an ultra-high vacuum was essential. The vacuum chamber consisted of a 6 inch stainless steel cube followed downstream by a large pumping station and other apparatus used in the MUBAR experiment. The SiO_2 powder was supported by a ramp shown in side view in the inset of figure 3.1. The support was a frame of Al with a rectangular piece of Al foil, of typical dimensions 5.5 cm $\times$ 11 cm $\times$ 0.12 mm, stretched across it at an angle of either 60° or 66° to vertical. The targets were made by sprinkling the SiO_2 powder onto the

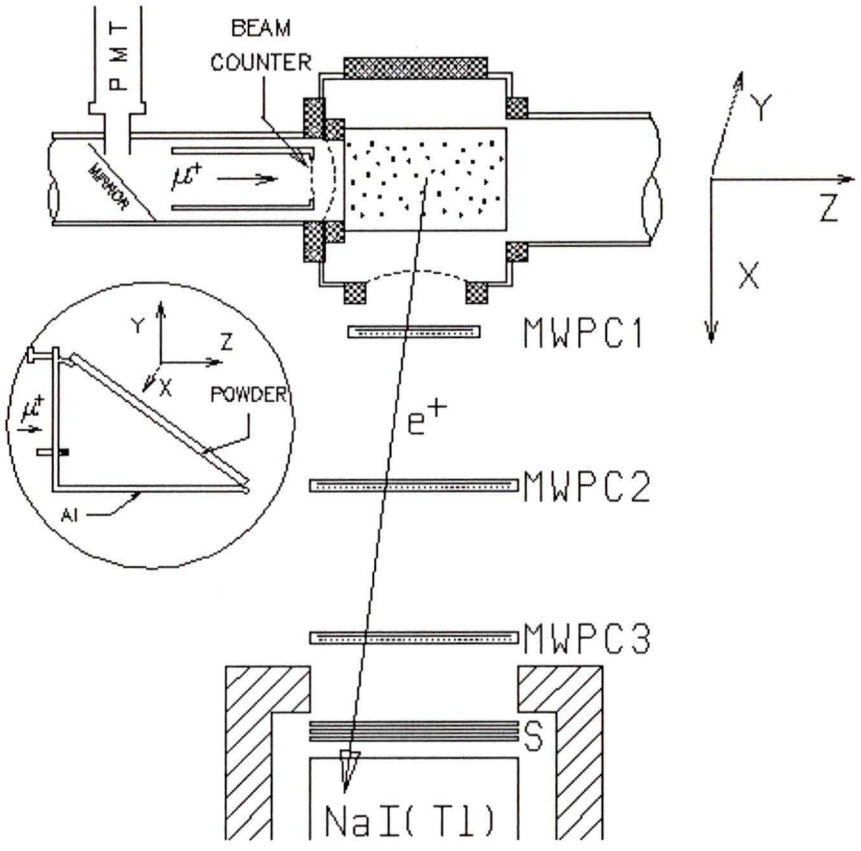

Figure 3.1: Schematic diagram of the apparatus to measure Mu yields. Dashed lines represent stainless steel vacuum windows. A side view of the target holder is shown in the inset.

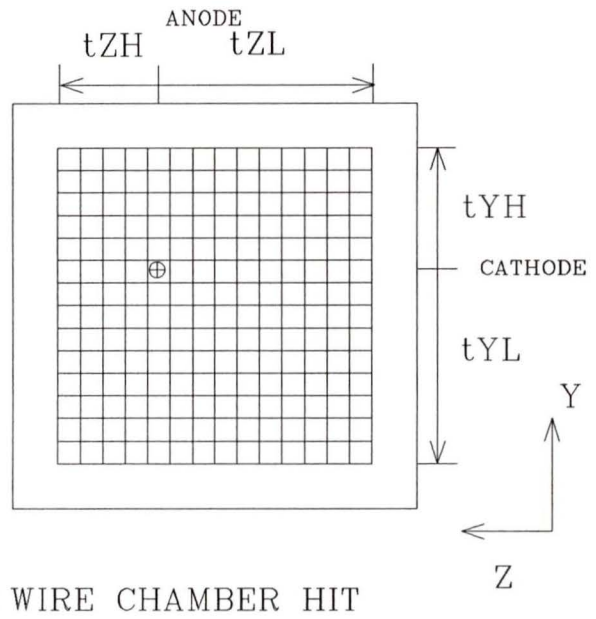

Figure 3.2: Schematic diagram of one wire chamber illustrating how it is used to obtain position measurements.

support ramp. The thickness of the powder was determined by weighing, and the entire target assembly was then suspended approximately in the middle of the cube.

The detection system included a telescope of three wire chambers. When a positron from a μ^+decay passes through the telescope the co-ordinates of the hits in all three chambers are recorded. A straight line trajectory is then calculated and extrapolated back to the target in the centre of the cube. This measures, relative to the target, the position of the decaying muon.

The wire chambers used were multiwire proportional chambers (MWPC's). Each chamber is a grid of fine wires at a voltage of ~4000 V. The chamber is sealed with two kapton windows and is filled with a mixture of isobutane and methanol, called "magic gas", characterized by a high gain. A position measurement is obtained from the chamber by using the relative differences in time for electrical signals to traverse the width of the chamber. A schematic diagram of one chamber is shown in figure 3.2. Cathode and anode wires

are arranged perpendicularly. A positron passes through the chamber, ionizes the gas and produces electrons which are collected by the anode wires. Signals from induced charges are also read from the cathode wires, making a position measurement in two dimensions possible. The wires in each grid are coupled to a delay line, so that the location of a hit is determined from a time signal. The time for the electrical signal to travel from the position in the grid through which the positron passed to the edge of the chamber along the positive z direction is recorded as tZH. Similarly the time for the signals to reach the other faces are also recorded. Then if the relationship between TDC channel and centimetres in space, called the dispersion, is known the co-ordinates of the hit in the wire chamber can be calculated as:

$$z = (tZH - tZL) \times \text{ z-dispersion } + \text{ z-offset}$$
$$y = (tYH - tYL) \times \text{ y-dispersion } + \text{ y-offset}$$

where the dispersions in the y and z directions are usually different, and the offsets are merely to define an arbitrary zero of the co-ordinate system.

The chamber dispersions were calibrated using a collimated ruthenium β source and an aluminium mask. The mask was an Al plate with a grid of holes very accurately drilled 1 cm apart. The mask was placed against the side of a chamber and the Ru source was passed across the holes, in 2 cm steps, in vertical and horizontal scans, see figure 3.3. So using the separation of the peaks in units of TDC channels the dispersions can be calculated. For example, for the chamber illustrated in figure 3.3 the dispersion is calculated to be 0.0963 cm/channel. From this calibration data the resolution of the wire chambers was also measured. The full width at half maximum (FWHM) of the point Ru source through the mask was 3.4 mm.

In the experiment, muonium atoms were detected by the passage of the muon decay positrons through the wire chamber telescope. For each of the three chambers a co-ordinate pair (y,z) of the positron hit was calculated.

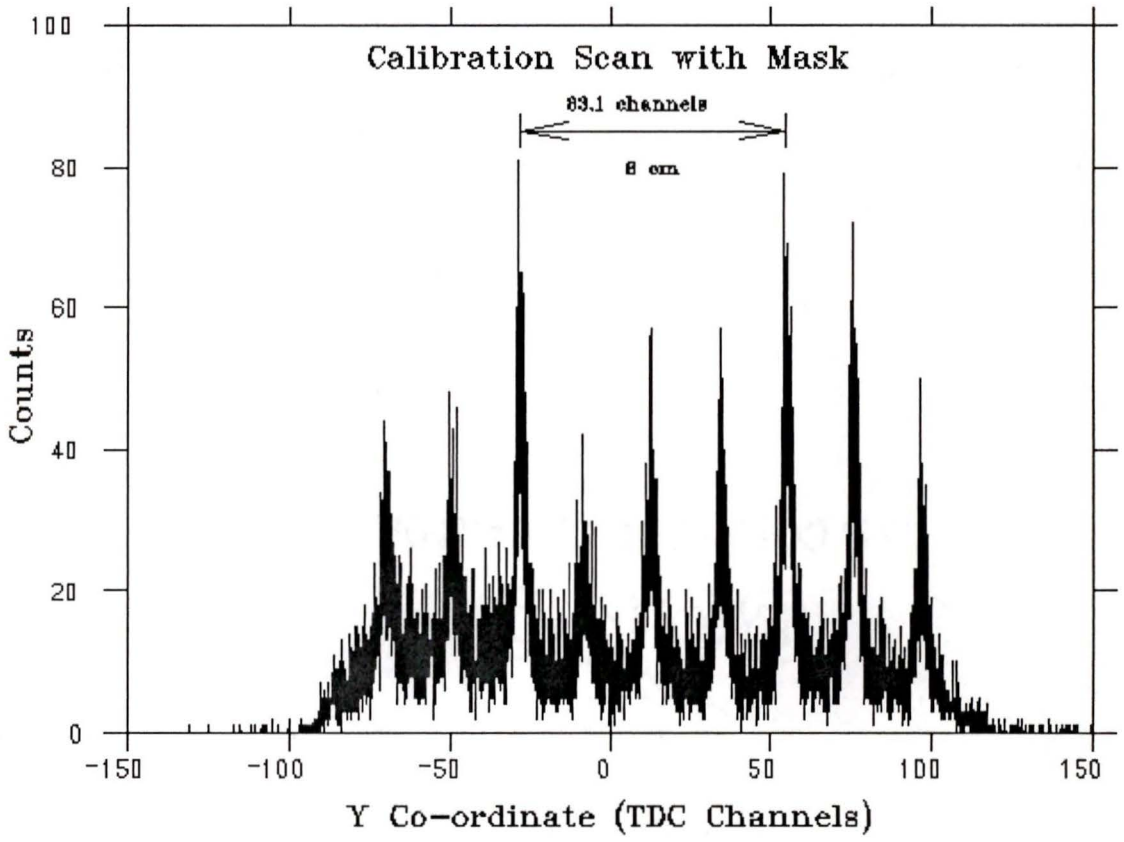

Figure 3.3: Figure showing the y co-ordinate of chamber 3. The peaks are from a Ru source being scanned across an Al mask in 2 cm steps.

The chambers were a fixed distance apart and the x co-ordinates were known. The (y,z) co-ordinates were then fit to a straight line using a least squares technique. This line, extrapolated to the plane x=0 gives the position of the decaying muon. The residuals from the linear fit also provide a way to fine tune the wire chamber dispersions calculated with the Ru source. The residual of the z co-ordinate of chamber 2, for example, is defined as:

$$\text{Res-z} = z - A - Bx$$

where A and B are obtained from the fit. Now if the dispersion of chamber 2 is set correctly, this residual should not depend upon where in the chamber the hit occurred. So a plot of Res-z should show no dependence on z. Figure 3.4 is a collection of scatter plots of Res-z verses z. In plot A the dispersion is too low and in plot C the dispersion is too high. With the dispersion set as in plot B the result is the optimum resolution from the wire chamber.

In addition to the wire chambers there was also a large NaI(Tl) crystal, the TRIUMF detector MINA, to measure the energy of the positrons. A characteristic Michel spectrum was clearly observed. In order to improve resolution, the MINA spectrum was also used to cut out low energy electrons which undergo large angle scattering at the stainless steel vacuum window. Three plastic scintillators, labeled S in figure 3.1, preceded MINA to ensure that it was measuring charged particles. In addition, one of these scintillators was used to time the muonium atom; the time of decay of a muon was determined by the difference in time between the beam counter scintillator and a scintillator preceding MINA.

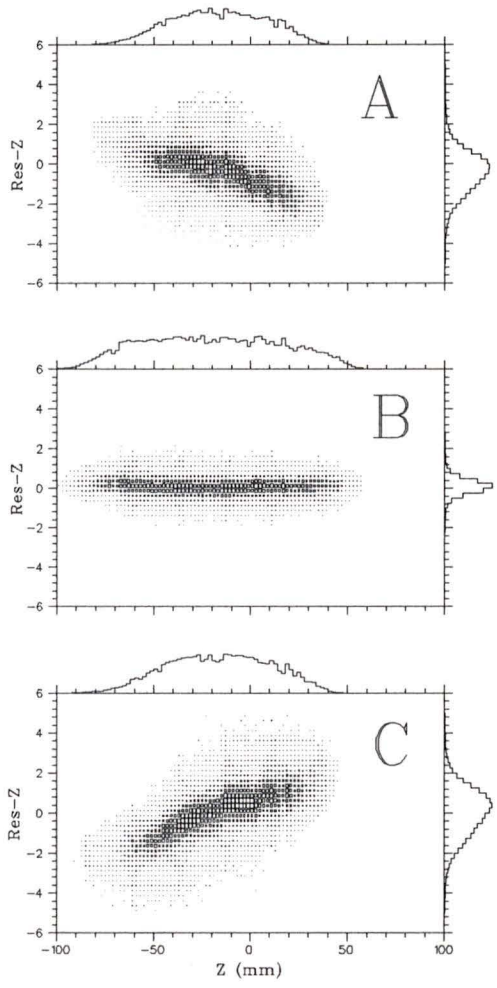

Figure 3.4: Scatter plots of Res-z verses z for slightly different z-dispersions.

Chapter 4

Experimental Procedure

Referring to figure 3.1 it is easily seen what constitutes an event in this experiment. An incoming muon fires the beam scintillator, called T. The muon stops in the target, decays and emits a positron in the direction of the wire chamber telescope. As was described earlier, each chamber produces four timing signals from which the co-ordinates of the hit in the chamber are calculated. The three scintillators S1, S2 and S3 also produce signals as does the NaI crystal, MINA. Figure 4.1 shows a circuit diagram of the on-line electronics used. Signals from each of the detectors are input from the left.

The rate of incoming muons was controlled so as to allow only one muon in the apparatus at a time in order to avoid confusion. The time of decay of a muon is the time difference between the firing of T and one of the S scintillators. If two muons fired T in quick succession it would not be known which decay positron belonged to which muon. Because signals could be "piled-up", the events for which T is fired a second time, that is before all of the signals due to the first muon are recorded, are cut from the data in software. Section A of figure 4.1 opens a gate which begins the event, EG, and sets a pile-up flag. Figure 4.2 is a schematic diagram showing the relative timing and gate logic comprising an event. The gate labels correspond to names on the logic units in figure 4.1. An event which would be cut due to pile-up is shown dotted.

Region	Condition on w_0 (mm)	Condition on v_0 (mm)
Target	$-5 \leq w_0 < 5$	$-50 \leq v_0 \leq 50$
R1	$5 \leq w_0 < 15$	$-50 \leq v_0 \leq 50$
R2	$15 \leq w_0 < 25$	$-50 \leq v_0 \leq 50$
R3	$25 \leq w_0 < 35$	$-50 \leq v_0 \leq 50$
R4	$35 \leq w_0 < 45$	$-50 \leq v_0 \leq 50$

Table 4.1: Table of definitions of the drift regions of the vacuum system

The event gate is open for 8μs, during which time the apparatus waits for decay positrons. Conditions which indicate a positron is present are a coincidence between the first wire chamber, all three S scintillators, and MINA. Section B in figure 4.1 looks for this decay positron signature. If this sequence is not observed in 8μs then the electronics are cleared and the system can accept another muon. If the sequence is observed then a hardware inhibit gate opens which inhibits the system from taking anymore events. The ETR signal generates a CAMAC LAM which interrupts the computer. CAMAC logic units are read and the event is written to tape. While doing this the computer produces its own busy signal; the output register, OR. Not until the OR is closed can data acquisition resume. This takes $\sim$ 1 ms. Section C in figure 4.1 sets the inhibit gates and clears the event.

In the data analysis a new rotated co-ordinate system (u,v,w) is defined from the co-ordinates (x,y,z) in figure 3.1. The rotation was performed about the x(u) axis by an angle equal to the tilt of the target so that the co-ordinate w was normal to the plane of the powder, see figure 4.3. For convenience of experimental set up both of these co-ordinate frames are left-handed.

Depending on the w and v co-ordinates, different regions of space were defined. If the calculated co-ordinates of a muon at the time of its decay were w_0 and v_0, then table 4.1 lists the different regions of space and their definitions. Of course, these definitions depend upon the zero of the w distribution being

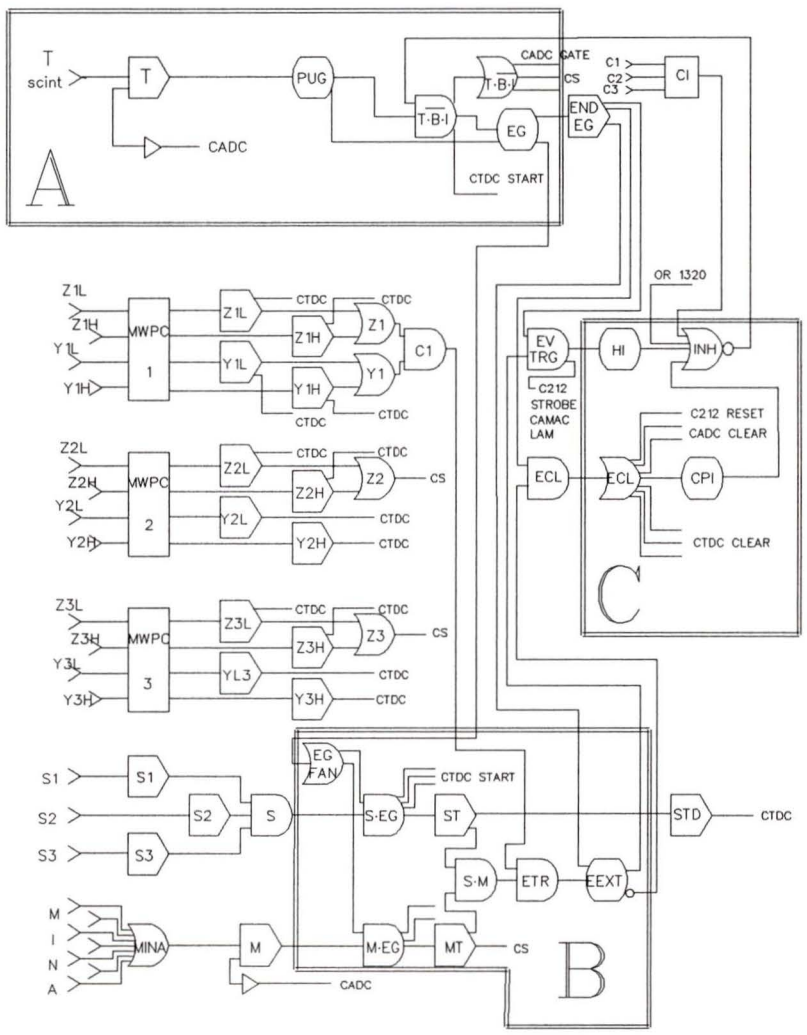

Figure 4.1: Circuit diagram of data acquisition electronics.

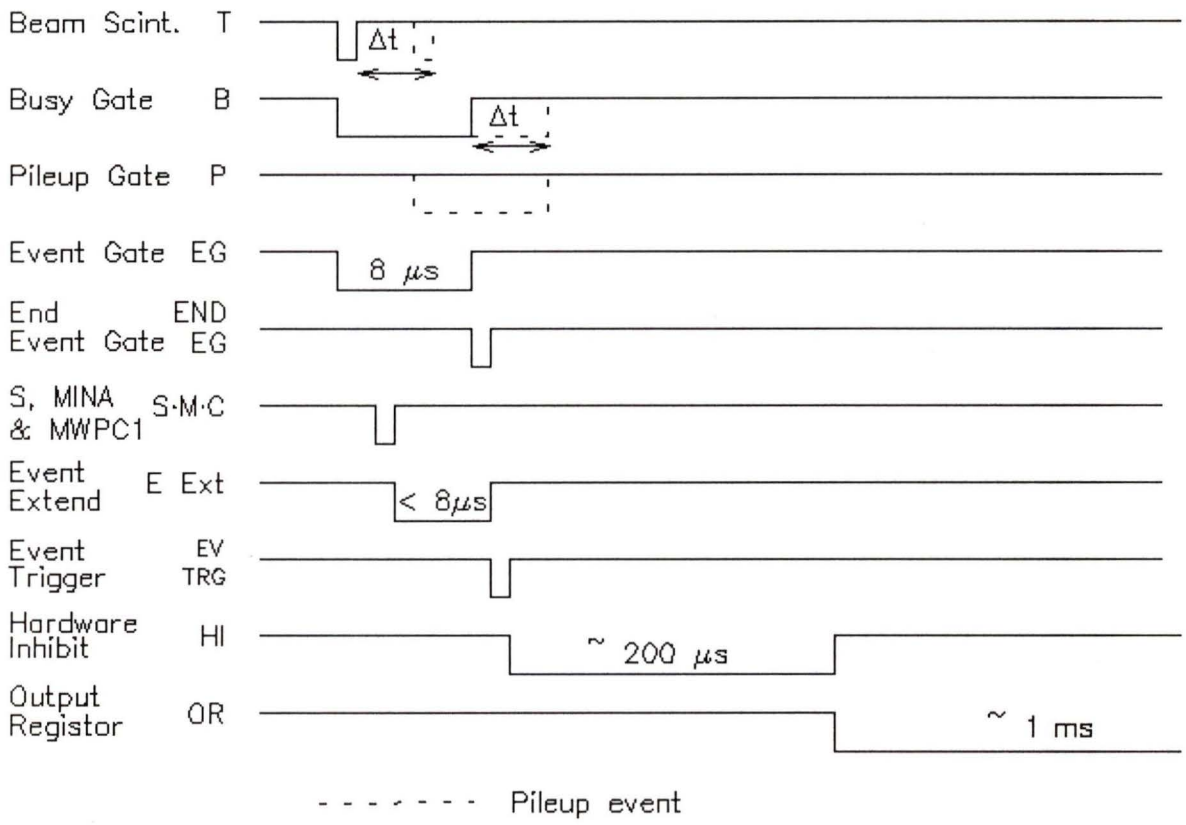

Figure 4.2: Diagram of event logic. Gate labels correspond to names of logic units in the on-line electronics diagram.

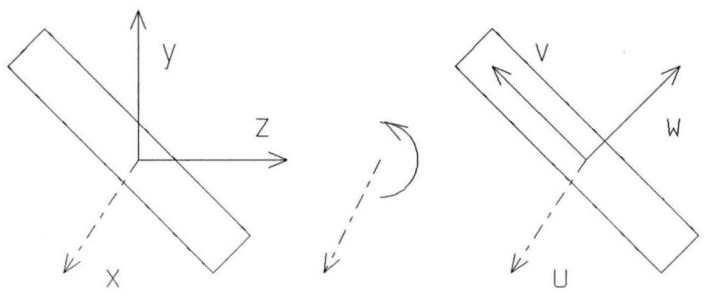

Figure 4.3: Diagram showing the definition of the rotated co-ordinate system. The rectangle is the target seen from the side.

consistently defined for each run. For this reason the mean of the counts seen coming from the target was carefully determined and, with an offset, was set to be at w=0. For each of these regions the time of decay was plotted. As will be discussed later, it was these time spectra which were used for the final Mu yield determination.

In addition to the hardware requirements outlined above, several cuts were also applied to the data in software to obtain the final sets of good events. Using the energy spectrum of the NaI(Tl) detector, MINA, low energy positrons were cut. This was because positrons of lower energies are more likely to undergo large angle scattering at the stainless steel vacuum window preceding the wire chambers, and so their trajectories would extrapolate back to an incorrect muon decay position. The cut was selected to be at the energy where the signal to noise ratio of the counts seen in R2 begins to level off at approximately 1:1. Although this MINA cut was not explicitly modeled in the Monte Carlo program that simulates the experiment, it is implicitly included in that

the resolution function of the detectors, which is modelled, depends on the value of the cut. Another cut similar in purpose to the MINA cut was a cut on χ^2 of the linear fit of wire chamber co-ordinates. A cut performed on the data that is also modelled in the Monte Carlo is a cut on the value of the slope of the straight line fit to the wire chamber hits. This cut limits the parallax uncertainties which arise when the positron trajectory is extrapolated back to the plane x=0.

Since the emission of muonium from the SiO_2 powder into the vacuum is a diffusion process it is advantageous to have as many μ^+'s as close to the surface of the powder as possible. For this reason the beam was ranged so that approximately half of the muons stopped in the powder and half went completely through and were lost. This was accomplished by sliding into the cube a rectangular piece of metal, called a catcher because of its purpose in the MUBAR experiment, 1.8 cm away from the target and parallel to it. The target and catcher were then imaged with the wire chamber telescope and the beam momentum was adjusted so that roughly half of the muons stopped in the target and half in the catcher. Figure 4.4 shows a plot so obtained, with the ratio of the target to catcher stops being 50:50.

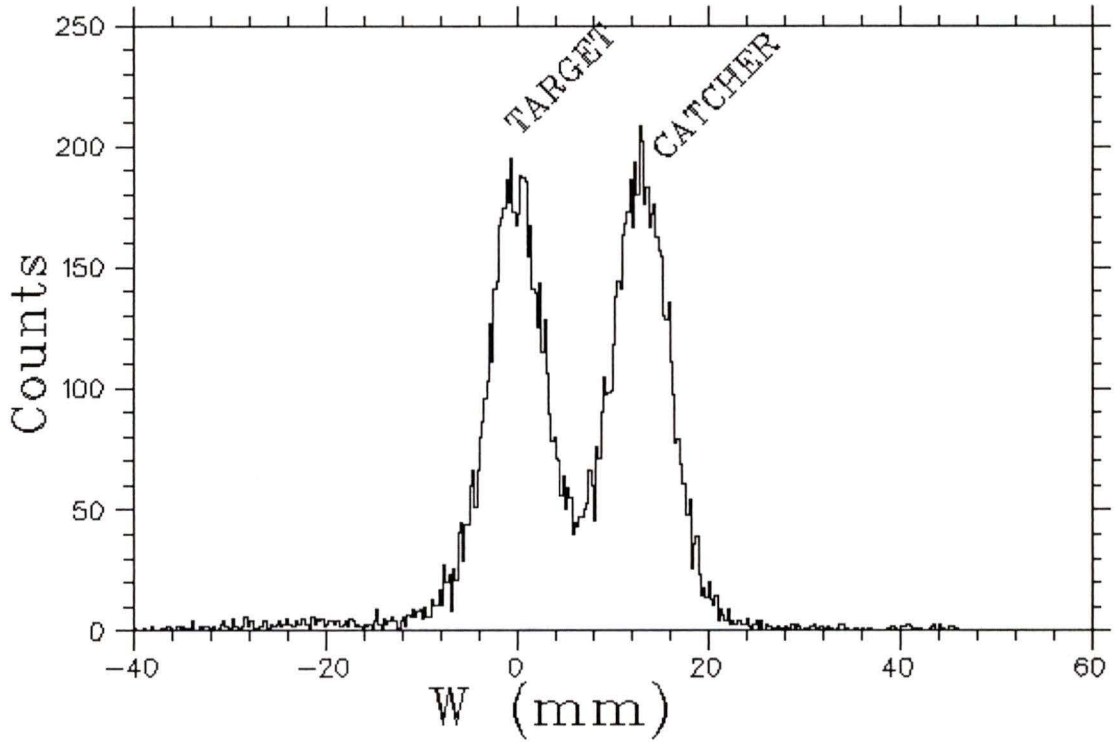

Figure 4.4: Plot of the w distribution of muon decays seen coming from the target and the catcher, used for ranging purposes. The beam momentum is adjusted to produce peaks of approximately equal size.

Chapter 5

Monte Carlo

The muonium yield from Cab-O-Sil can be calculated analytically if certain assumptions about the structure of the powder are made. Another approach, which relies on experimental measurement, is to treat the parameter of the model, the diffusion constant, as an essentially free parameter to be determined by comparison with data. The experiment was simulated by computer with the muonium generated according to the diffusion model. In addition, the simulation calculated the velocity and angular distributions of the muonium emitted into the vacuum. Then comparisons between the simulation and the data were made in order to fix model parameters, and finally the yield was calculated from the simulation.

As an alternative approach, it might be imagined that the yield could be determined independent of any particular model. The muonium atoms could simply be observed with the wire chamber telescope and counted. However, this approach is limited by detector resolution. The number of muonium atoms produced can never be counted exactly because there are always some which decay sufficiently close to the target that the decay positrons are detected to have come from the target and are not interpreted as having arisen from vacuum muonium. The Monte Carlo simulation is also used to calculate these corrections.

For this experiment a Monte Carlo program MUBEAM was used [26].

This program simulates the experiment from the point of the beam counter onwards. Muons are generated with an initial momentum, selected from a momentum distribution similar to that of the experimental beamline. They pass through successive "foils", including vacuum windows and defining apertures, as well as the powder target itself. Through each of these foils muons undergo energy loss and multiple scattering. After coming to rest in the target 61% of the muons become muonium and undergo a random walk out of the powder into the vacuum. The muons decay in one of the target, the vacuum, or the vacuum chamber walls and the decay positrons are projected into the solid angle seen by the wire chambers in the real experiment.

As the muon passes through each foil its range is reduced by an amount which depends on the foil's thickness and stopping power. This range is then corrected for range straggling effects. Straggling produces a spread the stopping positions of the muons with a standard deviation of:

$$\sigma_R = 0.0075\sqrt{\frac{1}{\epsilon(E_i)}}\frac{Z}{A}m_e c^2\left(R_i^{1.87} - R_f^{1.87}\right) \tag{5.1}$$

where Z is the atomic number of the foil material, A is its mass number, R_i and R_f are the ranges of the muon initially and after passing through the foil, and $\epsilon(E_i)$ is the ratio of the stopping power of the material to the stopping power of carbon at the initial energy E_i.

In addition to this standard range straggling effect, how far individual muons will travel in the powder will also vary due to non-uniformities in the thickness of the powder layer. For instance, a muon having a certain energy hits the centre of the powder target and stops near the surface. Another muon with the same initial energy hits the target closer to an edge where the powder layer is somewhat thinner and, whereas before the muon stopped, now the energy is sufficient to allow the muon to pass through the target. This second muon, of course, will not contribute to the thermal muonium yield.

The size of this non-uniformity effect depends on the condition of each individual target. The targets were made by sifting Cab-O-Sil onto a support ramp, which was hung at an angle of $\sim 66°$ and pumped down from atmosphere to a pressure of less than 10^{-6} Torr. Typically, targets were in the vacuum system, subject to vibrations due to vacuum pumps, for periods of days to weeks. Usually, small visible cracks and gaps formed.

The result of this effect is again an increase in the width of the muon stopping distribution in the target. This width was measured experimentally using the catcher ranging technique described earlier. The catcher was inserted and the momentum of the beam was scaled up and down by several percent. The scaling with momentum then, of the relative numbers of stops seen in the target and the catcher, is a measure of the stopping distribution width. The amount of total range straggling was adjusted in the Monte Carlo to reproduce this experimentally measured scaling behavior for each target.

For various targets, which were different sizes, thickness and at different angles, the scaling behaviour implied non-uniformities from 12 to 50% of the thickness. Considering the environment of the targets described above, this seems not unreasonable. However, an attempt was made at independently measuring the non-uniformity of powder layers. Using a solar cell and a laser, the variation in optical density was measured for two sample targets which were made in the same manner as the real targets. These targets were neither pumped down from atmosphere nor suspended at an angle for any period of time. However, this test does suggest that simply the making and handling of a target could result in a non-uniformity of 20 to 30% of the layer thickness over the central portion of the target.

In MUBEAM an effective multiple scattering angle is calculated once as

the muon leaves a foil using the formula: [27]

$$\theta_{rms} = \frac{19.94}{E_i + E_f}\sqrt{\frac{L}{L_R}}\left[1 + \frac{1}{9}\log_{10}\left(\frac{L}{L_R}\right)\right] \tag{5.2}$$

where E_i and E_f are the intial and final energies in passing through the foil, and $\left(\frac{L}{L_R}\right)$ is the effective thickness of the foil in radiation lengths. In order to more accurately model the distance through which the muon will travel in the power, the target foil is subdivided and treated as 10 individual foils thereby approximating large angle scatters by many smaller angle scatters.

The multiple scattering and range straggling portions of MUBEAM were tested experimentally using a μ^-beam. Negative muons were stopped in the middle of a stack of tungsten foils. Capturing of a $\mu^-$by a ^{184}W nucleus converts that nucleus to ^{184}Ta which decays with an 8 hour half life. By counting the induced activity in the individual W foils a profile of the μ^-beam was obtained. This profile agreed with the MUBEAM prediction.

Once the simulated muons stop in the SiO_2 powder 61% of them become muonium atoms in accordance with the μSR measurement. [19] These atoms must then undergo a random walk, in the framework of a Fickian diffusion model, to get out of the powder. This diffusion is a three dimensional process and should be modeled by a three dimensional random walk. However, a considerable simplification is possible since a 3-D random walk is equivalent to a 1-D random walk. For a 1-D walk with steps of variable size s_i, the probability density for a particle to travel a distance x after N steps is defined as:

$$\mathcal{P}_N(x) = \frac{1}{2\pi}\int_{-\infty}^{\infty} dk\, e^{ikx}\,[Q(k)]^N \tag{5.3}$$

where $Q(k)$ is the Fourier transform of the probability density distribution:

$$Q(k) \equiv \int ds\, e^{-iks} P(s) \tag{5.4}$$

and

$$P(s) = P(s_1)P(s_2)\cdots P(s_N) \tag{5.5}$$

is the probability of taking particular size steps s_i. For steps of equal length a:

$$P(s) = p_+\delta(s-a) + p_-\delta(s+a). \tag{5.6}$$

If the particle is equally likely to step forwards as backwards then $p_+ = p_- = \frac{1}{2}$. The rms distance that a particle can be expected to travel in N steps of length a is:

$$(x)_{rms} = \sqrt{N}a. \tag{5.7}$$

The general definition of $\mathcal{P}_N(x)$ can easily be extended to three dimensions:

$$\mathcal{P}_N(\mathbf{r}) = \frac{1}{(2\pi)^3}\int d^3\mathbf{k}\, e^{i\mathbf{k}\cdot\mathbf{r}}\,[Q(\mathbf{k})]^N \tag{5.8}$$

where

$$Q(\mathbf{k}) = \int d^3\mathbf{s}\, e^{-i\mathbf{k}\cdot\mathbf{s}}P(\mathbf{s}) \tag{5.9}$$

for variable vector steps $\mathbf{s}$. It is here that the simplification occurs. Mohling [28] outlines a proof which shows that the 3-D probability density is equivalent to a 1-D probability density:

$$\mathcal{P}_N(\mathbf{r}) = \mathcal{P}_N(r). \tag{5.10}$$

Also, for vector steps of equal length a, the rms distance a particle undergoing a 3-D random walk can be expected to travel in N steps is:

$$(|\mathbf{r}|)_{rms} = \sqrt{N}a. \tag{5.11}$$

The problem is now reduced to one of modelling 1-D diffusion with a 1-D random walk.

The solution of the one dimensional diffusion equation is:

$$W(x) = \frac{1}{\sqrt{4\pi Dt}}\exp\left[\frac{-x^2}{4Dt}\right]. \tag{5.12}$$

If this diffusion is to be modelled by a random walk with uniform steps of length a then an expression for $\mathcal{P}_N(x)$ corresponding to this walk can be found using the distribution (5.6) and equations (5.3) and (5.4):

$$\mathcal{P}_N(x) = \frac{1}{\sqrt{2\pi N}a} \exp\left[\frac{-x^2}{2Na^2}\right]. \tag{5.13}$$

Comparing this equation to (5.12) gives the correspondence between the diffusion parameters and parameters associated with the random walk simulation:

$$\frac{1}{4\pi Dt} = \frac{1}{2\pi Na^2} \Rightarrow D = \frac{N}{t}\frac{a^2}{2}. \tag{5.14}$$

Now if d is the thickness of the SiO_2 powder target and n is the number of steps it takes to cross it, usually $n \sim 100$, then:

$$a = \frac{d}{n}. \tag{5.15}$$

If Δt is the increment of time used in the random walk then:

$$N = \frac{t}{\Delta t} \tag{5.16}$$

where t now has the interpretation as the time required to diffuse across the entire powder layer.

And so a random walk with uniform steps of sizes

$$a = \frac{d}{n}$$

and time steps of size

$$\Delta t = \frac{a^2}{2D}$$

will model a diffusion process governed by the diffusion constant D.

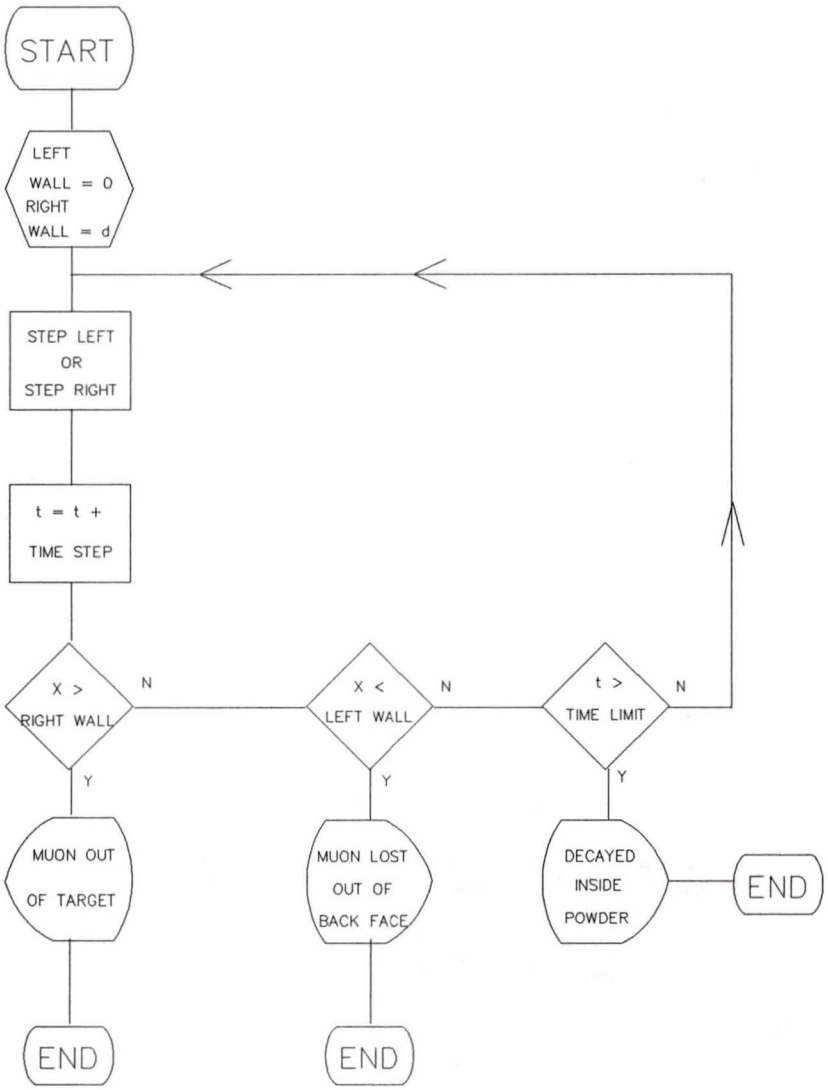

Figure 5.1: Flow chart of random walk simulation in MUBEAM.

Figure 5.1 shows a flow chart of the random walk simulation in MUBEAM with step sizes selected as above. At the end of this procedure one of three things will have happened: a Mu atom will have diffused to the surface of the powder layer and escaped into the vacuum, or the muon will have decayed inside the target while diffusing, or the muon (or Mu atom) will have reached the back face of the powder in which case it is considered to have decayed in the target since adjacent to the back face is the Al support ramp which the muon certainly won't have enough energy to cross.

Once the muonium atom reaches the surface of the powder target it is emitted into a vacuum drift space. Figure 5.2 is a flow chart of this portion of MUBEAM. The Mu is given a random velocity selected from a Boltzmann distribution at a temperature of 300 K, and a $\cos\theta$ angular distribution, where θ is defined with respect to a normal to the powder. Since the Mu atoms are emitted from a plane the angular distribution can be expected to be analogous to Lamberts law in optics. The validity of the assumption of a $\cos\theta$ angular distribution was tested by considering a uniform distribution instead. For each of these angular distributions, the v-distribution of the diffusing muonium was compared to the data in region 2. Backgrounds were subtracted from the data using a nitrogen gas subtraction technique described in chapter 6. The v-distribution in R2 is well described by a Gaussian and a $\cos\theta$ angular distribution produced a v-distribution of $\sigma = 16.9 \pm 0.3$ mm, whereas a uniform angular distribution implied $\sigma = 18.5 \pm 0.4$ mm. The errors quoted here are statistical only. The v-distribution of the experimental data is described by a Gaussian of width $\sigma = 17.1 \pm 0.7$ mm implying that the angular distribution of muonium emission is more consistent with a $\cos\theta$ than with a uniform distribution. The ϕ distribution is assumed to be uniform. In MUBEAM there is also a facility for simulating the introduction of a gas into the vacuum drift space. Experimentally, N_2 gas is introduced into the vacuum system as a way of measuring backgrounds. In the simulation the Mu atom elastically scatters

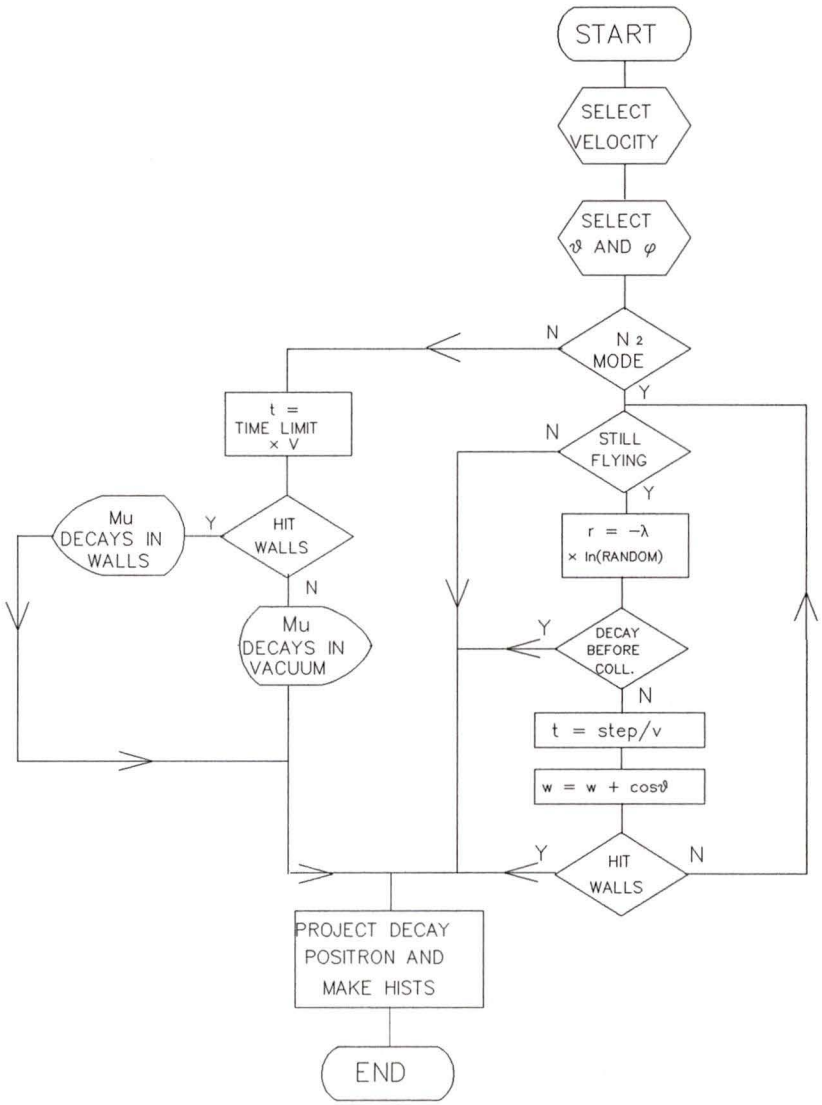

Figure 5.2: Flow chart of simulation in MUBEAM of the evaporation and travel of a Mu atom into the vacuum.

off of large spheres with a mean free path, λ, that is an input parameter.

The particular mean free path used is, of course, related to the pressure of the gas introduced. The mean free path of Mu atom in an ideal gas is: [24]

$$\lambda = \frac{1}{\pi n d^2} \tag{5.17}$$

where d is the distance of closest approach, and n is the number of atoms per unit volume. For an ideal gas at 1 atm. and 0° C the concentration of atoms is known as the Loschmidt number:

$$n_0 = 2.69 \times 10^{19} \text{ atoms/cm}^3. \tag{5.18}$$

The concentration then is:

$$n = 2.69 \times 10^{19} \left(\frac{P}{760}\right)\left(\frac{273}{T}\right) \tag{5.19}$$

where T is the temperature in K, and P is the pressure in Torr. For $P = 1$ Torr and $T = 300$ K:

$$n = 3.22 \times 10^{16} \text{ atoms/cm}^3. \tag{5.20}$$

The distance of closest approach can be approximated by the sum of the radii of a Mu atom and a N_2 molecule. The Bohr radius of a Mu is:

$$r_{Mu} \sim 0.4 \times 10^{-8} \text{ cm}$$

and the radius of a N_2 molecule is: [25]

$$r_{N_2} = 1.6 \times 10^{-8} \text{ cm}.$$

So then

$$d \sim 2 \times 10^{-8} \text{ cm}$$

and the mean free path of a Mu atom in 1 Torr of N_2 is:

$$\lambda \sim 0.02 \text{ cm}.$$

For each muon decay a positron track is generated into the solid angle subtended by the wire chamber telescope in the real experiment. Experimentally this track is blurred due to the detector resolution. The resolution function is modelled in MUBEAM but, as will become apparent in the next chapter, because of the method of fitting the simulated data to the real data, the final yield parameters obtained are not very sensitive to this function.

When the simulated muon finally decays then, its co-ordinates in the vacuum system are known as is its history: was it indeed a muonium or just a muon, did it escape from the powder, did it hit the walls of the chamber, etc. The vacuum system is again divided into different regions depending on the w co-ordinate of the decay positrons, and histograms similar to those of the experimental data are made. What would correspond to one timing histogram of experimental data would be four histograms depending on whether the muon decayed in flight, in the target, in the walls of the chamber, or as a vacuum muonium atom. From these one can deduce the correction to the number of vacuum muonium atoms which are directly counted and which could not be sufficiently resolved with the detectors alone.

Chapter 6

Investigation of Mu Yield

The determination of the muonium yield was made by a comparison between the Monte Carlo simulation and the data in a region of the vacuum chamber relatively far from the target. Figure 6.1 shows a density plot of the number of muon decays, in space, as calculated by the extrapolation of decay positron trajectories. The definitions of these regions in space were given in table 4.1. In order to minimize the effect of background from target muon decays, region 2 was selected for comparison to the Monte Carlo. This region had a signal to noise ratio of between 1 and 0.35 depending on changes made to the experimental apparatus for the MUBAR experiment.

For each of the regions R1, R2, R3, and Target, the time of decay of the muons was plotted. Figure 6.2 shows these time spectra for each of the four regions. The muonium signal can be seen as a nonexponential time dependence introduced by the motion of muonium into and out of the different regions.

An average velocity can be calculated by dividing the distance of the muon from the target by the time of decay. An additional correction due to the time acceptance of the apparatus was incorporated into the Monte Carlo through the modelling of the experimental geometry. Figure 6.3 shows a plot of a typical velocity spectrum along with a histogram of the spectrum which is predicted by the Monte Carlo. The agreement is good indicating thermal emission. In addition, no change in yield is noted when an electric field of

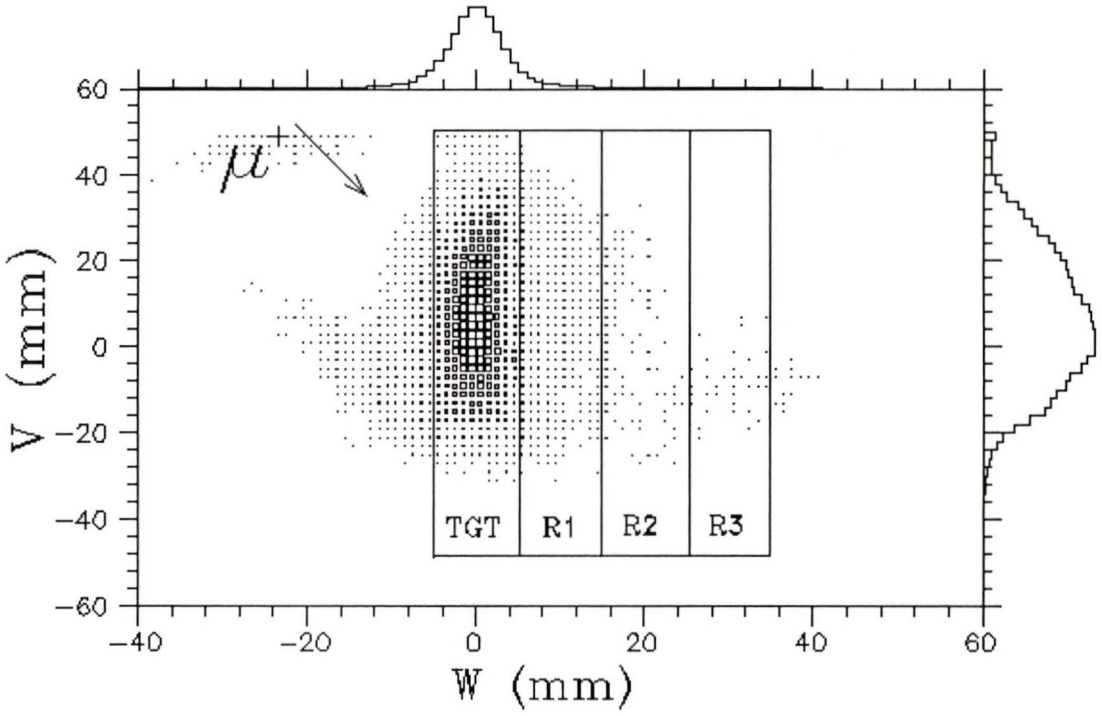

Figure 6.1: Density plot of position of muon decays in space. Yield was determined on the basis of analysis of region 2.

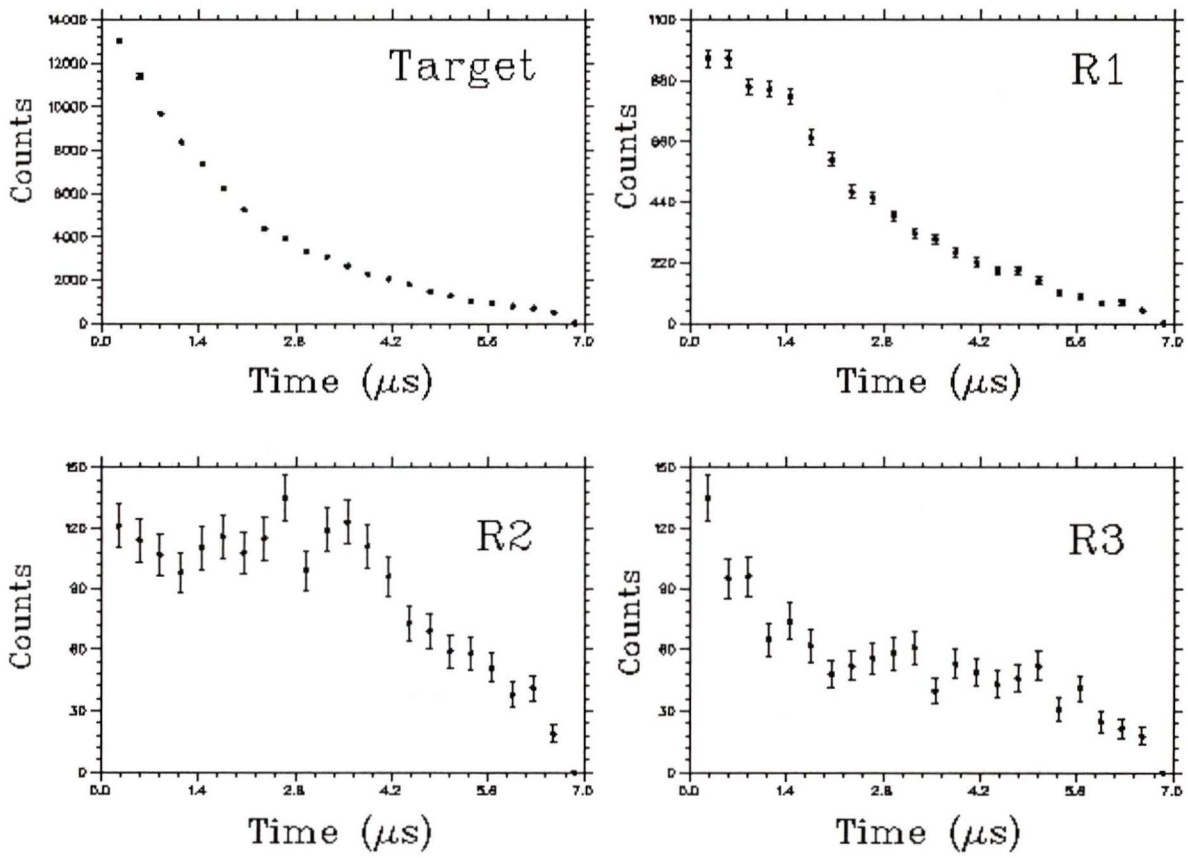

Figure 6.2: Muon decay times for various spatial regions.

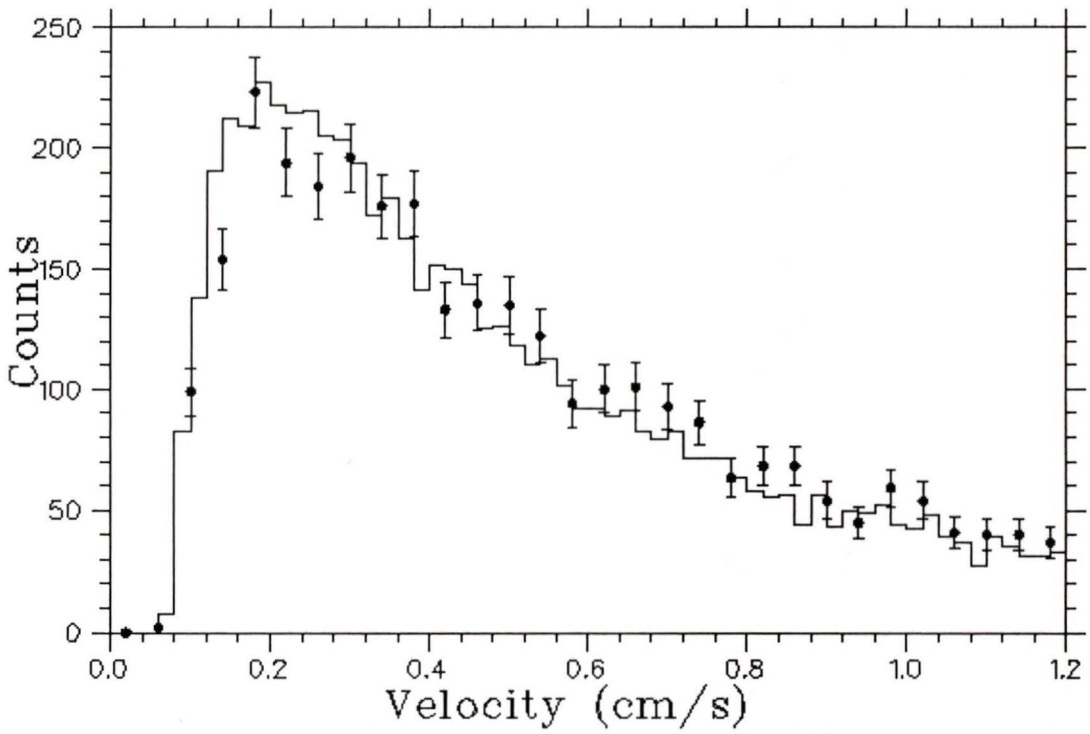

Figure 6.3: Velocity spectrum of muonium with histogram of the spectrum predicted by the Monte Carlo.

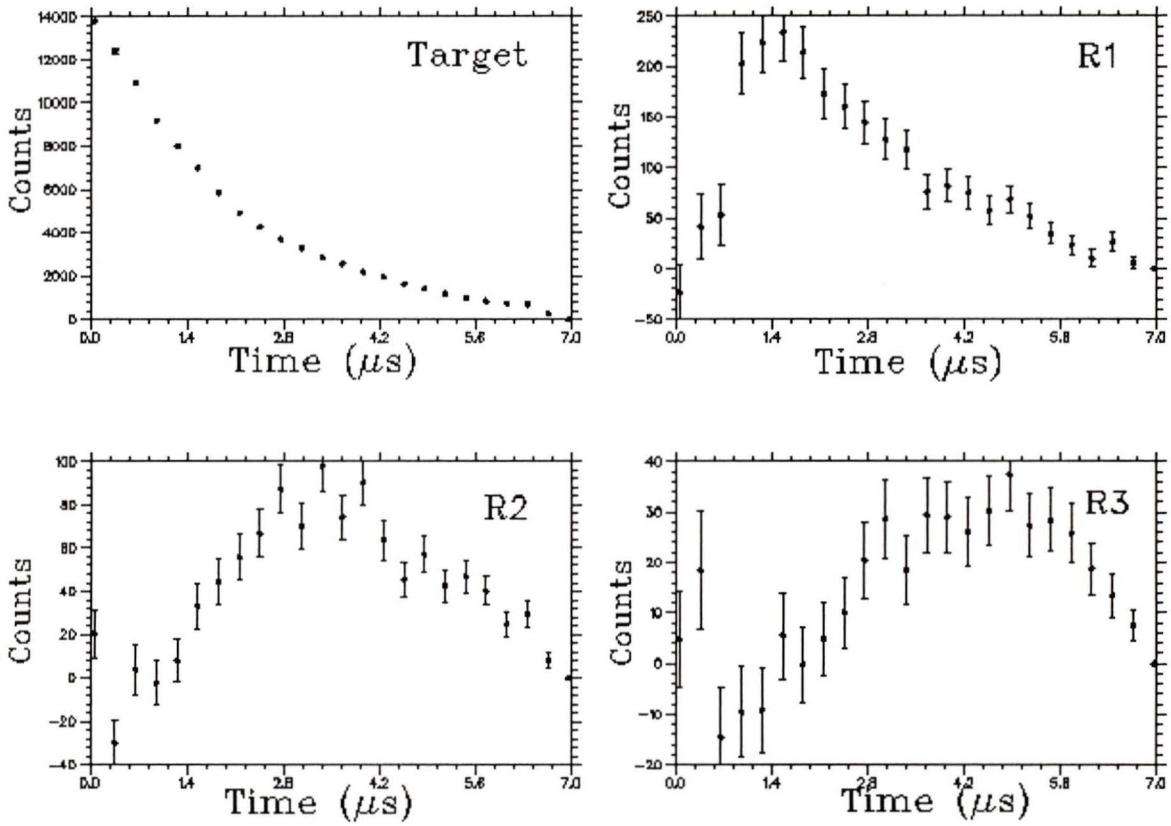

Figure 6.4: Muon decay times for spatial regions now with the background due to decays from the target subtracted.

2.5 V/cm is applied [23]. This confirms the neutral nature of the signal.

In addition to muonium signal, however, each of the three vacuum regions contains a background from target muon decays being misinterpreted, due to detector resolution, as having come from another region. This background has a μ^+-lifetime exponential time dependence and so can easily be subtracted. Figure 6.4 shows the same four spectra but with this background subtracted. Now the thermal muonium signal can be clearly seen.

An experimental background test was also done to determine if sources of background other than the one mentioned above had a significant effect.

Nitrogen gas, at a pressure of $\sim$ 1 Torr, was introduced into the vacuum chamber and additional data was taken. The nitrogen suppresses the escape of thermal Mu from the target but does not affect the background from such sources as μ^+ stops in the walls of the chamber and the target. When this data taken in nitrogen is subtracted from the data taken in vacuum, the spectra shown in figure 6.4 are obtained.

To calculate the yield of Mu, comparison between the experimental data and MUBEAM simulated data is made with the decay time spectrum of region 2. This spectrum is fit with a μ^+-lifetime background and a muonium signal component each multiplied by a free parameter. The signal component is the corresponding Monte Carlo calculated histogram containing, however, only those counts which in the simulation originated from thermal muonium.

The computer simulated data is normalised to the experimental data in such a way that if the diffusion constant in the Monte Carlo is correct then the simulation will have predicted precisely the amount of signal which is seen. On the other hand, if the diffusion constant is not quite correct, more or less muonium is required and the muonium signal parameter in the fit will be greater or less than 1. In this way the yield, which is a measured quantity, can be determined without full knowledge of the diffusion constant, which is a quantity of the diffusion model. In fact, once the fit is made and the yield calculated, the diffusion constant which describes the process, assuming all other model parameters remain fixed, is also determined.

So the basic procedure, then, of determining the Mu yield is as follows. The spectrum of muon decay times in vacuum region 2 is fit with a background component, measured to have a μ^+ lifetime, and a thermal muonium signal, calculated from MUBEAM. Once the relative size of these components is known, the Monte Carlo is used to calculated the total yield, given a particular amount of muonium in region 2 of the vacuum chamber. In addition,

since the diffusion constant which will produce a particular yield is unique, this diffusion constant is now also fixed. More discussion of the diffusion model itself will follow in a later chapter. Figure 6.5 shows a typical R2 spectrum and the resulting fit. Plot A shows both components, plot B shows only the background component and plot C shows only muonium with the background having been subtracted.

Contributions to the uncertainty in the determination of the yield fall into three general categories: statistical fluctuations, uncertainties involved in selecting Monte Carlo parameters, and uncertainties in the method of fitting the yield to the Monte Carlo.

The uncertainty in the yield due to statistical fluctuations in the data is calculated in the fitting process and has values which range from 5 to 30% depending on the run.

In the Monte Carlo program there are several "free" parameters which must be adjusted to reproduce various features of the data. The features of the data to be reproduced include the size of the beam spot on the target, and the amount of range straggling present in the target due to powder inhomogeneities. Also, since the computer simulated vacuum system is also divided into regions, for comparison to R2 of the data, the co-ordinate offsets must be the same for both data and simulation. The quoted uncertainties were determined by varying the Monte Carlo parameters a small amount and finding the resulting change in the yield. Since these parameters are determined by direct comparison with some aspect of the experimental data, the amount by which the parameters were varied corresponds to a reasonable estimate of how well that aspect of the data was known. For example, in all cases the co-ordinate offset in the data agreed with the offset in the Monte Carlo to within 0.4 mm. Changing the Monte Carlo offset by 0.4 mm results in a 10% difference in the yield measurement. In the case of the target inhomogeneity factor, a conservative estimate of the uncertainty was determined using the MUBAR data for

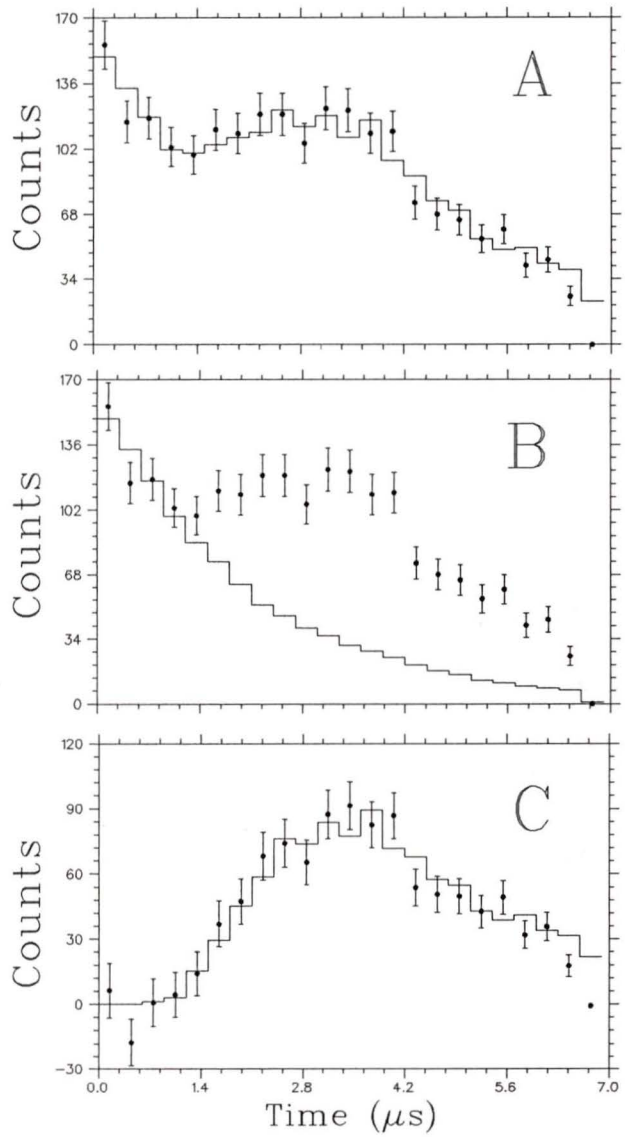

Figure 6.5: Typical R2 spectrum with the histogram being the fit to the Monte Carlo. Plot A has both components, plot B shows the background component, while plot C shows only the muonium signal with the background having been subtracted.

which this factor was the least well known. For these targets the parameter could only be determined to within approximately 18%. Changing the parameter in the Monte Carlo by this amount produces a 10% variation in the yield. The variation produced in the diffusion constant is considerably higher and will be discussed in chapter 7. The combined uncertainty then, from what might be called setting up the Monte Carlo program, was 17%

Other uncertainties are introduced by the way in which the data was fit to the Monte Carlo. For example, R2 was selected as the comparison vacuum region. If another region, say R3, has been selected the total yield calculated would now be based on the amount of muonium in R3 and would have been slightly different due to statistical fluctuations. Also, the Monte Carlo simulated data had to be normalised somehow to the real data. Possible normalisations include the total number of events passing all cuts, the number of incident muons, or the number of stops seen in the target. Selection of a particular normalisation again introduces fluctuations into the calculated yield. The combined variation introduced by these fitting method effects is 14%.

So the total uncertainty in the determination of the muonium yield varies from 22 to 38% depending on the statistical uncertainty.

One of the primary uses for muonium is in the search for muonium conversion to antimuonium. As part of this search it is, of course, necessary to calculate the yield of muonium produced. The MUBAR group at TRIUMF has recently reported an upper limit on Mu conversion based on data taken in November 1987 [7], and is in the process of analysing data from a second longer run completed in the summer of 1988. Calculation of muonium yields for these two searches has been one of the primary motivations for this work.

The experimental configurations were virtually identical for the 1987 and 1988 runs. The only significant differences being the tuning and ranging of the beam. In 1988 tuning and ranging were done with the cube in place (see figure 3.1). For tuning, a small plastic scintillator was inserted in the

centre of the cube in place of the target, and the spot size of the beam was minimized. Ranging was done by inserting the catcher next to the target and, with beam momentum, adjusting the relative numbers of stops in both. In 1987, in order to perform other tests related to the MUBAR experiment, tuning and ranging were without the cube in place. The beam focus was only approximately located in the centre of the cube, and ranging was done by inserting material into the beam and measuring the range width of the beam. As a result of tuning, the beam spot on the target was approximately 9% larger in 1987. With the 1987 method of ranging the catcher data, which was necessary to estimate the width of the stopping distribution in the target, was not taken. This width depends on target inhomogeneities and since the physical targets and methods of powder layer preparation were identical, the target inhomogeneity for the 1987 data was taken to be the same as that for 1988.

The targets themselves consisted of an Al support ramp of dimensions 5 mm $\times$ 13 mm $\times$ 0.119 mm, suspended at an angle of 66° to vertical. The average powder layer thickness was 8.6 mg/cm^2. In order to produce the maximum amount of muonium the target was made as large as possible. As a result a portion of the target, $\sim \frac{1}{3}$ of the length, was out of the field of view of the wire chambers. This experimental geometry was incorporated into MUBEAM which corrected for the fact that a portion of the important vacuum region R2 was out of the field of view. In order to check this correction, a target was constructed which was similar except that the size was only 4.5 mm $\times$ 8 mm and it was suspended at 60°. With this target the entire region R2 was visible with the wire chambers. The yields of the 60° target, which will be discussed further below, were consistent with those of the 66° target indicating that the geometrical correction was not a source of systematic error.

For both the 1987 and 1988 MUBAR targets the beam momentum was

p = 28.5 MeV/c. The momentum width was set to one of either 10% of p, referred to as the wide momentum bite, or 3% of p, referred to as the narrow momentum bite. Table 6.1 lists the yields calculated for each run of yield data collected, as well as a weighted average for each target. The uncertainties quoted in these measurements were calculated as outlined above.

The yield measurements taken at various times for various MUBAR targets were also examined for any evidence of a decrease in the yield with time, which could result from a deterioration of the powder layer, for example. The yields were fit as a function of the amount of time the targets were in the vacuum system when the data was taken. No evidence of any trend was found.

For an experiment such as MUBAR it is of interest to produce as much muonium in the vacuum chamber as possible. From table 6.1 it can be seen that, to within uncertainties, the total yield of Mu per incident muon is the same for narrow and wide momentum bite. That this is true could be due to the effect of target inhomogeneities increasing the width of the stopping distribution in the target. Since this widening is combined in quadrature with the width already present due to the momentum bite, the target inhomogeneity produces a relatively larger effect in the narrow momentum bite configuration than with a wide momentum bite. The weighted mean of the yields for each of the wide and narrow momentum bites is (1.9 ± 0.2) % of the incoming muons. Since the momentum width is controlled by the opening and closing of slits in the beam pipe, the maximum number of μ^+'s and thus the maximum number of Mu atoms are obtained with a wide, or 10%, momentum bite.

In order to maximise the Mu production it is also important to know how the yield depends on the depth into the powder at which a muon stops. The muon beam in this experiment was ranged so that half of the muons stopped in the target and half went completely through and were lost. The reasoning behind the procedure is that since the emission of Mu is thought to be a diffusion process, it is advantageous to have as many muons stopping as close

Run	Date	SiO_2 mg/cm^2	$\frac{\Delta P}{P}$ %	Yield / tgt stop %	Yield / inc. μ^+ %
115	1987	8.5	10	4.2 ± 1.0	2.4 ± 0.6
116	1987	8.5	10	2.6 ± 0.7	1.5 ± 0.4
117	1987	8.5	10	3.8 ± 1.0	2.2 ± 0.6
118	1987	8.5	10	3.8 ± 0.9	2.2 ± 0.5
Weighted mean			10	3.4 ± 0.4	2.0 ± 0.2
119	1987	8.5	3	4.3 ± 1.1	2.2 ± 0.6
120	1987	8.5	3	4.4 ± 1.2	2.3 ± 0.6
Weighted mean			3	4.3 ± 0.8	2.2 ± 0.4
314	1988	9.1	3	5.3 ± 1.3	2.5 ± 0.6
315	1988	9.1	3	2.3 ± 0.9	1.1 ± 0.4
Weighted mean			3	3.3 ± 0.7	1.5 ± 0.6
348	1988	9.1	10	4.8 ± 1.1	2.6 ± 0.6
362	1988	8.7	10	4.5 ± 1.1	2.5 ± 0.6
369	1988	8.7	10	2.3 ± 0.6	1.2 ± 0.3
370	1988	8.7	10	2.6 ± 0.7	1.4 ± 0.4
Weighted mean			10	2.7 ± 0.5	1.4 ± 0.3
387	1988	8.3	10	3.8 ± 0.9	2.1 ± 0.5
406	1988	8.4	3	5.2 ± 1.2	2.5 ± 0.6
441	1988	8.4	3	4.3 ± 1.0	2.0 ± 0.5
Weighted mean			3	4.7 ± 0.8	2.2 ± 0.4
407	1988	8.4	10	4.5 ± 1.1	2.4 ± 0.6
442	1988	8.4	10	5.9 ± 1.6	3.2 ± 0.9
443	1988	8.4	10	5.1 ± 1.3	2.8 ± 0.7
Weighted mean			10	4.9 ± 0.9	2.6 ± 0.5

Table 6.1: Yields calculated for targets used in the MUBAR experiment in both 1987 and 1988 runs. The weighted means were calculated using the total uncertainty including both statistical and systematic contributions.

Run	SiO_2 mg/cm^2	P MeV/c	$\frac{\Delta P}{P}$ %	Fr. in Target	Yield / tgt stop %	Yield / inc. μ^+ %
72	13	24.3	10	0.56	7.5 ± 1.9	4.1 ± 1.0
79	13	24.3	3	0.56	7.9 ± 1.9	4.4 ± 1.1
80	13	23.8	3	0.67	6.2 ± 1.7	4.2 ± 1.1
87	13	23.2	3	0.80	2.9 ± 0.8	2.3 ± 0.7
82	13	22.6	3	0.90	1.5 ± 0.5	1.3 ± 0.5
86	13	21.8	3	0.96	0.5 ± 0.5	0.4 ± 0.4
458	17.9	28.2	10	0.51	4.5 ± 1.0	2.4 ± 0.6
459	17.9	28.2	3	0.51	7.4 ± 1.7	3.7 ± 0.8
460	17.9	27.9	3	0.61	6.5 ± 1.5	4.0 ± 0.9
461	17.9	27.6	3	0.71	5.1 ± 1.2	3.6 ± 0.8

Table 6.2: Yields obtained with beam momentum scans on two targets to probe the yield as a function of stopping depth in the powder. Included is the fraction of incident muons which stop in the target at specific momenta as calculated by the Monte Carlo.

to the surface of the powder as possible so as not to have too much material through which the muons must diffuse. To examine this effect more closely, yield data was taken at several different beam momenta, effectively probing the muonium yield as a function of the stopping depth in the powder. The data was taken in a MUBAR run of 1988 and in a development run in 1986.

The target of the 1988 data is the 60° target described above with a thick Cab-O-Sil layer of 18 mg/cm^2. The 1986 target was of dimension 4.5 mm × 7.5 mm, also suspended at an angle of 60° to the vertical, and had a powder thickness of 13 mg/cm^2. While both data sets in the momentum scan were taken with a narrow (3%) momentum bite, the 1988 beam momentum was ∼ 28 MeV/c and the 1986 momentum was ∼ 24 MeV/c. Table 6.2 lists the data which was taken in 1986 and 1988 including the momenta, momentum bite, and the fraction of incident muons which stopped in the target. For each target one run was taken at wide momentum bite for comparison with the MUBAR targets. Also listed are the muonium yields both per incident muon

and per muon stopped in SiO_2 . In figure 6.6 both of these yields, determined from the narrow momentum bite data of varying momenta, are plotted as a function of the fraction of the beam which stopped in the target. From these plots it can be seen that while the yield per SiO_2 stop steadily decreases as the beam is stopped further back into the powder, the total Mu yield reaches a maximum not at a 50% fraction but rather at approximately 60% of the beam stopped. The reason for this is the combination of two competing effects which are responsible for the total yield. Firstly, in order for a Mu to be produced, a muon must stop in the Cab-O-Sil. It follows that more stops in the SiO_2 will increase the amount of muonium produced in the target. However, the muonium must also diffuse out of the powder, and the probability of getting out decreases with the depth into the layer at which the Mu atom is formed. Therefore in order to produce the maximum yield of Mu per incident muon, the beam should be ranged so that 60% of the muons stop in the target and the rest pass straight through.

Another target which was studied was a very thin target with 2.8 mg/cm^2 of Cab-O-Sil. The yield per target stop for this target was $(15.9 \pm 3.6)\%$ for a narrow momentum bite and $(15.0 \pm 3.6)\%$ for a wide momentum bite. The yields per incident muon were $(7.6 \pm 1.7)\%$ for narrow and $(5.8 \pm 1.4)\%$ for wide momentum bite. These are consistent with results measured previously with a similar target [23]. That these yields are higher than the yields from the thicker targets could again be due to the relative size of the powder inhomogeneities. Say, for example, that making a powder target introduces a variation in the thickness of the layer of $\sim$20 %. In absolute terms this corresponds to a smaller number of grams per square centimeter for a thin target than for a thick target. So the stopping distribution in a thick target will contain a greater amount of widening which results in more muons stopping further from the surface of the layer.

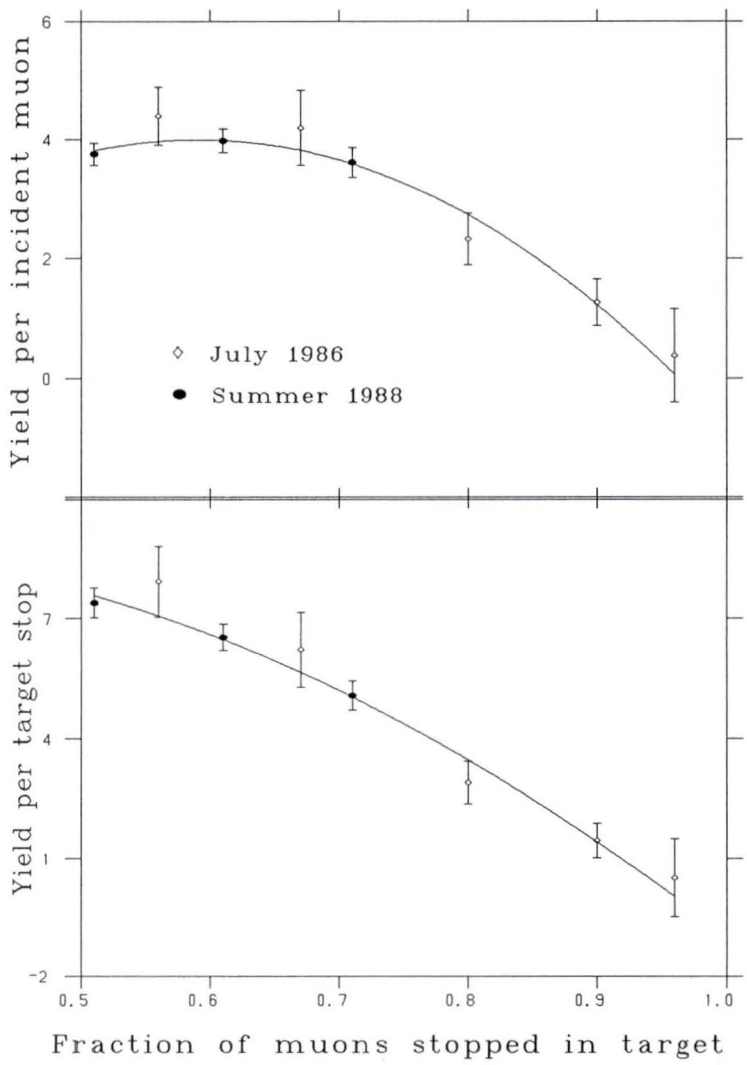

Figure 6.6: Plots of muonium yield per stop in the powder, and per incident muon as a function of the fraction of the muon beam which stops in the target.

In order to measure the backgrounds in this experiment nitrogen was introduced into the vacuum chamber. The dependence of the Mu yield on gas pressure has been studied in connection with this background estimation. Using the thin target of 2.8 mg/cm^2, different pressures of nitrogen were introduced into the chamber and the yields were measured at each pressure. Figure 6.7 shows the Mu yield per SiO_2 stop as a function of N_2 pressure. At a pressure of $\sim$ 1 Torr the thermal Mu signal is completely quenched. This quenching of yield with N_2 is also a measure of the cross section of the collision of Mu atoms with N_2 molecules. Using the yield from vacuum region 2 and MUBEAM, the mean free path of the Mu atoms was calculated for each pressure of N_2. Then equation (5.17) can be used to obtain a value for the distance of closest approach, d. Using the Bohr radius of a Mu and the radius of a N_2 molecule, a geometric estimation of 2×10^{-8} cm was calculated. Quenching the yield with 6 mTorr of N_2 implied a value for d of $(1.9 \pm 1.0) \times 10^{-8}$ cm, and using 20 mTorr of N_2 implies a distance of $(2.5 \pm 1.2) \times 10^{-8}$ cm. Both of these are consistent with the above approximation.

Yield measurements with other physical forms of SiO_2 were performed in order to better understand what properties of Cab-O-Sil allow it to produce such a large amount of muonium. No yield was observed from a Cab-O-Sil target which had been compressed [23], indicating that the microscopic structure of a material, and not just its chemical composition, is an important property in determining whether a material will produce muonium in vacuum.

Another form of SiO_2 which was investigated was Opti-Pur made by Merck. This is an extremely pure crystalline powder of SiO_2 developed for use in the manufacture of optical fibers. While it is dense compared with Cab-O-Sil, having a density of 0.51 g/cm^3, it has a surface area of 600 m^2/g which exceeds that of Cab-O-Sil. The total yields from this powder are (1.9 ± 0.5) % for a wide momentum bite and (1.8 ± 0.4) % for a narrow momentum bite. Both

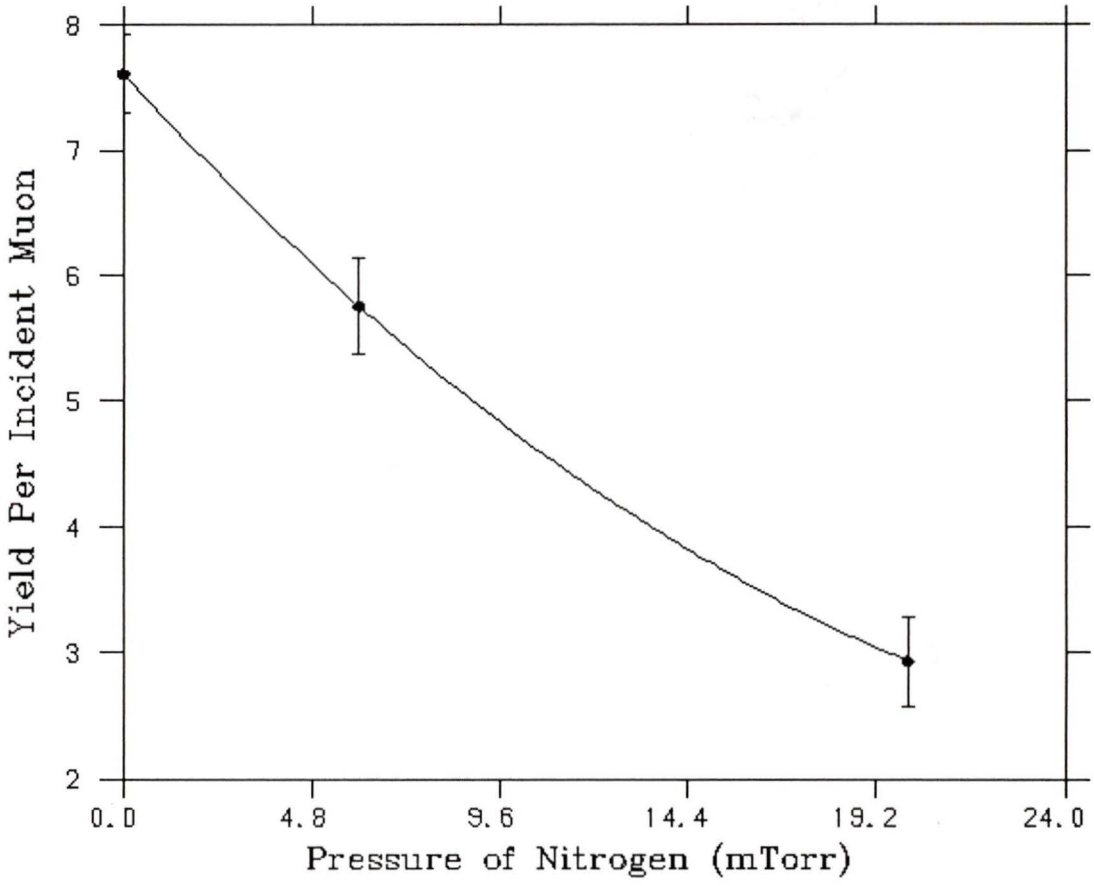

Figure 6.7: Muonium yield per stopped muon as a function of nitrogen pressure in the vacuum chamber. Background measurements were taken at a pressure of 1 Torr.

measurements were taken at a beam momentum of 28.5 MeV/c. These yields are comparable to those from Cab-O-Sil.

A form of low density SiO_2 is aerogel. This is a silica gel which has been dried under high gas pressures so it keeps its form instead of collapsing in on itself. It has a density of 0.136 g/cm^3, and a high surface area of typically 500-800 m^2/g depending on the density [29,30]. The form of aerogel is a solid translucent block which was cut to a convenient size with a sharp knife. The aerogel target was tried but it proved to be a poor producer of Mu, giving a yield per incident muon of only (0.7 ± 0.2) % with narrow momentum bite. An attempt was made at cleaning the surface of the aerogel by bleeding $\sim$ 20 mTorr of O_2 into the vacuum chamber and sparking a plasma. The yields after this procedure were further reduced by approximately 50 %.

By considering the aerogel and Merck targets it is apparent that a measurement of a single quality of a material, such as density or surface area, is not sufficient to predict the muonium production capability of that material. While like Cab-O-Sil, aerogel is also composed of chains of silica particles of small diameters, these chains are crosslinked to produce a sort of skeletal support for its solid form. In Cab-O-Sil the chains are entwined but not firmly connected. Another characteristic which is important for aerogel is pore size. The type of aerogel used would have a maximum pore size of $\sim$20 nm. However, exposure to moisture preferentially decreases size of the largest pores [30] by as much as a factor of 4 in some cases. The macroscopic structure is not changed nor is the measured surface area. This could perhaps explain the reduction in yield following plasma cleaning.

Recently Woodle et al. [31] at SIN have also measured the yield of thermal muonium from Cab-O-Sil. An incident beam of 20.1 MeV/c and width 1.5 Mev/c was used. The target thickness was 9.0 mg/cm^2. The yields obtained for EH5 were (18 ± 2)% of the stopped muons and (11 ± 2)% of the in-

coming muons. The diffusion constant was calculated to be (1068 ± 81) cm^2/s. The apparatus used was quite similar but no data which is directly comparable was collected by the MUBAR group. To make a comparison, a Monte Carlo simulation was run using the diffusion constant inferred from this work, 620 ± 80 cm^2/s, in the configuration of the SIN experiment. When the target was assumed to be perfectly homogeneous the simulated yields calculated were (8.2 ± 0.4)% of the incident muons, or (17 ± 1)% of the stops in the Cab-O-Sil. If, however, the targets were assumed to have an inhomogeneity of 30% of the target thickness, comparable to the targets used in this work, then the simulated yields were (4.9 ± 0.3)% of the incident muons, or (9.9 ± 0.6)% of the stops in the Cab-O-Sil. The errors quoted represent the uncertainty in the above diffusion constant. The variation in the simulated yields gives an indication of the importance of considering the target inhomogeneity in the modeling of the stopping distribution in the target.

Chapter 7

Determining a Diffusion Constant

All of the yield determinations in this work have been made in the context of a diffusion model which obeys Fick's Law. It can be asked whether such a model is valid. If emission of muonium from Cab-O-Sil is a Fickian diffusion process then the diffusion constant governing the process should be unique, depending only on the physical characteristics of the powder's structure. This means that all of the yields obtained, for different target configurations and beam momenta, should be predicted by the same diffusion constant.

For each yield calculated it is possible to extract from the Monte Carlo a diffusion constant which would predict that yield. Table 7.1 lists all of the configurations for which yield data was taken, and the diffusion constant which the calculated yield implies in each case. Figure 7.1 shows a plot of these diffusion constants as a function of the mean stopping depth into the powder in millimeters. The error bars plotted indicate both the statistical and systematic errors discussed previously. A weighted fit to these points yields a value of (620 ± 80) cm^2/s with $\chi^2_\nu = 1.1$. While the errors on the diffusion constants obtained are large, the data do seem to be consistent with a constant value.

Difficulty in precisely determining the diffusion constant should not be linked to a similar lack of knowledge of the muonium yield however, since the diffusion constant is much more sensitive to the internal parameters of

Run	Date	SiO_2 mg/cm^2	P MeV/c	$\frac{\Delta P}{P}$ %	Mean Depth (mm)	D cm^2/s	$+\Delta D$ / $-\Delta D$
72	1986	13	24.3	10	0.51	1600	800 / 600
79	1986	13	24.3	3	0.28	1390	620 / 510
80	1986	13	23.8	3	0.53	1470	730 / 590
82	1986	13	22.6	3	1.34	840	420 / 350
87	1986	13	23.2	3	0.90	870	390 / 320
148	1987	2.8	22.0	3	0.45	370	220 / 180
149	1987	2.8	22.0	10	0.50	440	280 / 240
458	1988	17.9	28.2	10	2.54	825	220 / 220
459	1988	17.9	28.2	3	1.78	1020	460 / 370
460	1988	17.9	27.9	3	2.01	1160	510 / 420
461	1988	17.9	27.6	3	2.29	1220	540 / 450
MUBAR	1988	8.6	28.5	10	1.56	690	290 / 290
MUBAR	1988	8.6	28.5	3	1.38	320	160 / 160
MUBAR	1987	8.6	28.5	10	1.71	580	250 / 250
MUBAR	1987	8.6	28.5	3	1.53	570	275 / 275

Table 7.1: Different target configurations and incident muon beam momenta for which yield data was taken and the diffusion constant determined.

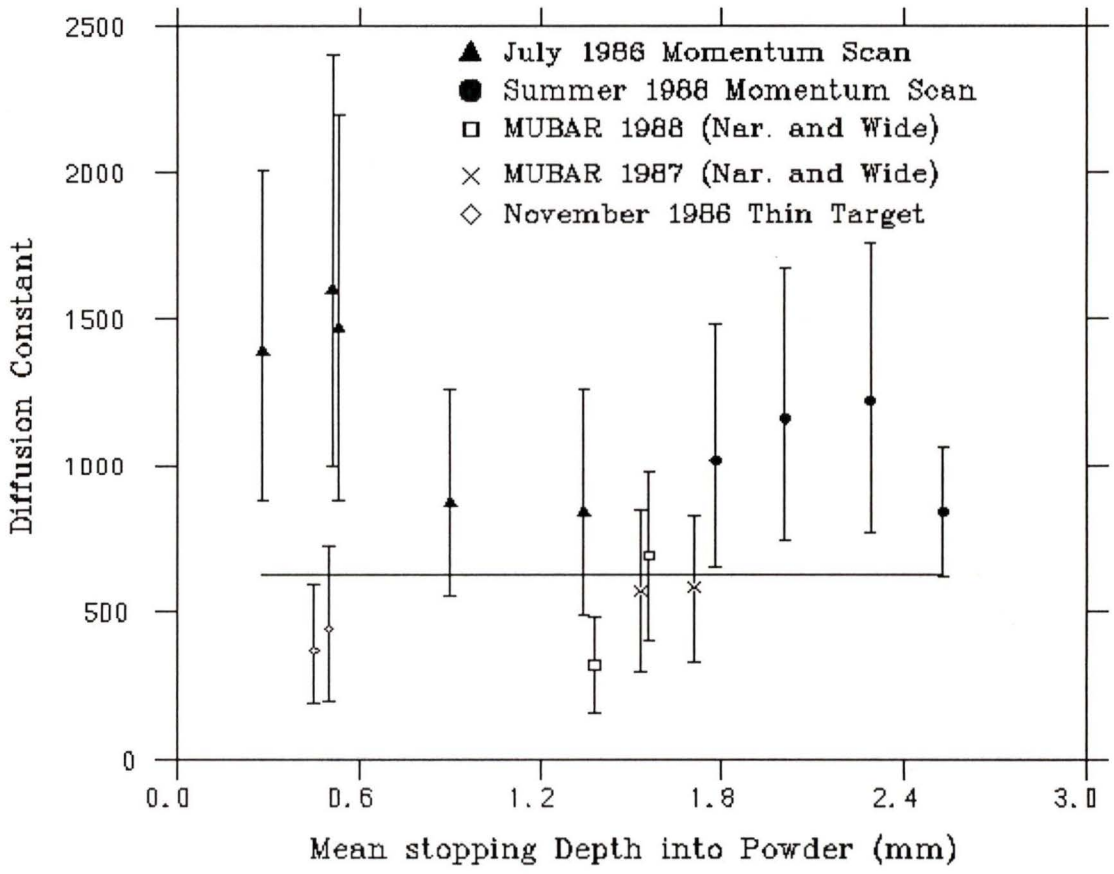

Figure 7.1: Diffusion constants, for different target configurations and muon beam momenta, which are implied by the muonium yields.

the model. The method of yield fitting which uses a free parameter diffusion constant results in yield measurements which are to a much greater extent independent of the precise stopping distribution in the target. For extraction of a diffusion constant governing the process, however, the shape of the stopping distribution is critical.

The variety of stopping distributions represented in figure 7.1 is actually quite substantial. The diffusion constants are plotted against the mean stopping depth in the powder. However, this quantity is really a combination of several experimental configurations which determine the shape of the stopping distribution. The momentum bite of the incident muon beam is primarily responsible for the width of the target stopping distribution. Figure 7.2 shows the typical difference in stopping distributions between narrow and wide momentum widths. For each target, yield data was taken at both widths. In all cases the diffusion constants with the two configurations are consistent.

The momentum of the incident muon beam is also important in determining the stopping distribution. As the momentum is decreased, more muons are stopped further back into the powder. Two sets of data were taken in which the beam momentum was varied (see table 6.2). Figure 7.3 shows the largest difference in the stopping distribution which was considered. Again, the diffusion constants calculated with these distributions are consistent with one another.

Given an incident momentum and momentum bite, the single most important parameter determining the target stopping distribution is the target inhomogeneity. This is measured experimentally using the catcher and varying the momentum of the beam. However, a complete momentum scan was not always taken for each 1988 MUBAR target and for the 1987 MUBAR data the catcher method of ranging was not even used. The stopping width was determined for two of the five MUBAR targets which were used in 1988. An average stopping width was then used for all of the MUBAR targets, both

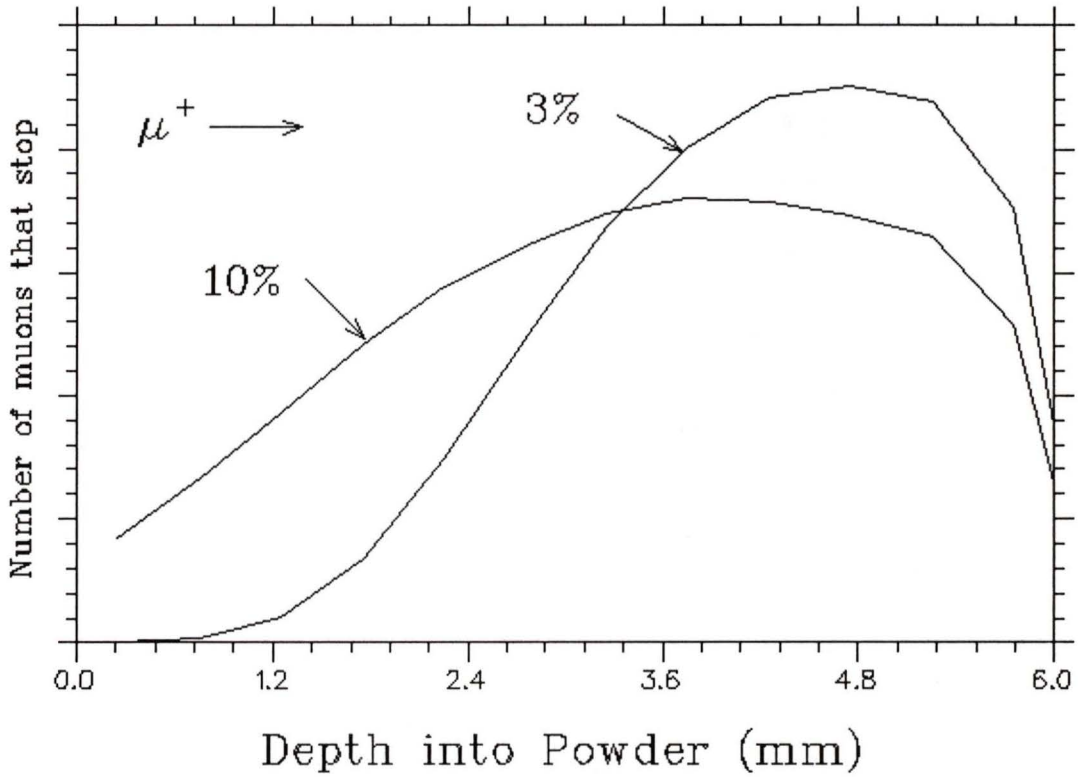

Figure 7.2: Distributions of stops in the target calculated in the Monte Carlo for 3% and 10% momentum bites.

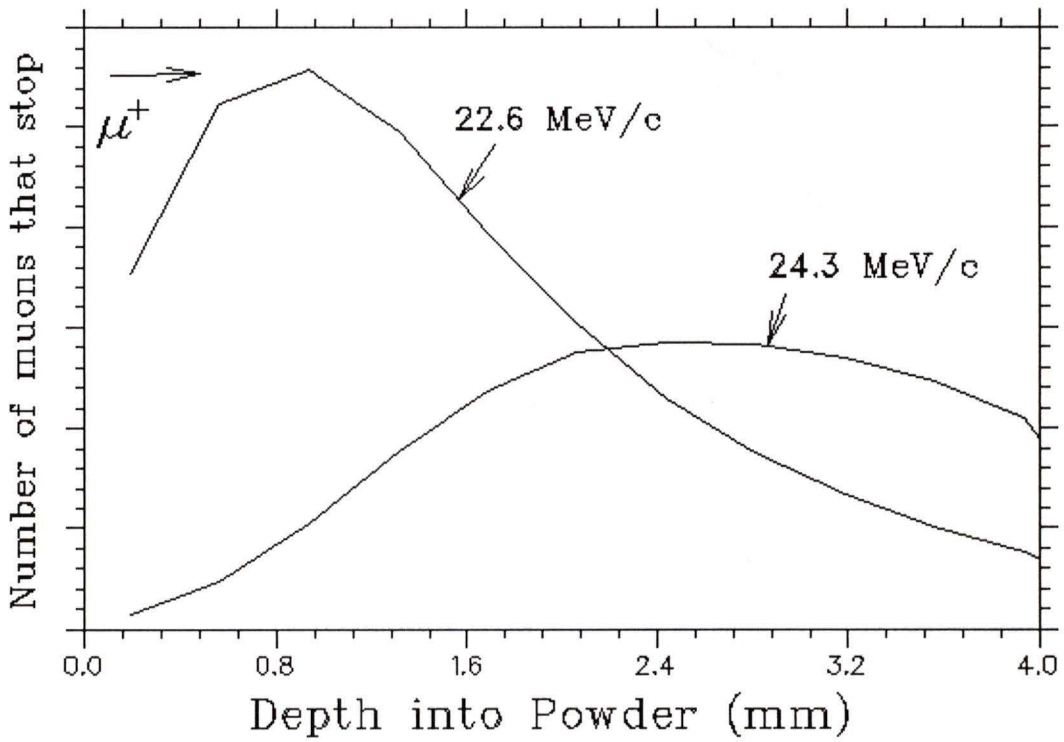

Figure 7.3: Plots showing the largest difference in target stopping distribution considered due to changing the incident muon momentum.

1987 and 1988. As was mentioned previously, the inhomogeneity for these targets could only be determined to approximately 18%. Varying the parameter by this amount in the Monte Carlo produces a 40% change in the diffusion constant which is determined. This additional uncertainty is included in the diffusion constant measurements for the MUBAR targets only. For the other targets more complete sets of catcher ranging data were taken and so the inhomogeneity parameter was determined much more precisely.

The only exceptions are runs 148 and 149, the thin target runs, for which no catcher ranging data was taken. Since the target is so thin it is less sensitive than thicker targets to the width of the stopping distribution. However, a large statistical uncertainty for these runs combined with the lack of catcher ranging data make these data points no more reliable in the determination of the diffusion constant than the points from other targets.

The present analysis of muonium production from Cab-O-Sil is consistent with a Fick's Law diffusion model for each target examined. However, variations of the diffusion constant of up to a factor of 2, correlated to the condition of the target, cannot be excluded. In addition, while the vacuum yields are experimentally well determined, the diffusion constant depends quite sensitively on the modeling of the stopping distribution, which is difficult for a material like Cab-O-Sil.

Conclusions

In this work various aspects of muonium production were studied. In the area of production technique it was found that the selection of an appropriate material depends not only on measurements of surface area or density but on the microscopic structure of the particular form of silica. Once the material is selected, Cab-O-Sil in this case, the optimum yield is obtained when approximately 60% of the incident muons are stopped in the target. Due to

the relative size of the effect of the inhomogeneity of the target layer, higher yields are obtained with thinner targets. As for the properties of the muonium thus produced, it was found that the atoms are emitted at thermal velocities consistent with a $\cos\theta$ angular distribution.

It was also determined in this work that the emission of muonium from Cab-O-Sil is consistent with a Fick's Law diffusion model. This is significant considering that previous work [23] noted inconsistencies in the diffusion constants for different target thickness and muon beam configurations. The change that made a consistent description possible was the modelling in the Monte Carlo of the inhomogeneity that existed in the powder layer. This had the effect of increasing the total amount of range straggling of incident muons and thus changed considerably the shape of the stopping distribution in the target.

The diffusion constant which was obtained is an effective value which is meant to describe the many different processes in Cab-O-Sil which are involved in the production of muonium. This diffusion constant is substantially larger than that suggested by an analytical calculation assuming a uniform distribution of spheres of silica. This implies some sort of enhancement in the mean free path of the muonium atoms due to the arrangement of the SiO_2 spheres, which again indicates that the microscopic structure must be considered when explaining muonium production.

Bibliography

[1] V.W. Hughes and T. Kinoshita, in *Muon Physics*, edited by V.W. Hughes and C.S. Wu, Academic, New York, 1977, Vol. 1, p. 12.

[2] F.G. Mariam, W. Beer, P.R. Bolton, P.O. Egan, C.J. Gardner, V.W. Hughes, D.C. Lu, P.A. Souder, H. Orth, J. Vetter, U. Moser, and G. zu Putlitz, *Higher Presicion Measuremnt of the hfs Interval of Muonium and of the Muon Magnetic Moment.* Phys. Rev. Lett **49** (1982) 993.

[3] D.E. Casperson, T.W. Crane, A.B. Denison, P.O. Egan, V.W. Hughes, F.G. Mariam, H. Orth, H.W. Reist, P.A. Souder, R.D. Stambaugh, P.A. Thompson, and G. zu Putlitz, *New Precise Value for the Muon Magnetic Moment and Sensitive Test of the Theory of the hfs Interval in Muonium.* Phys. Rev. Lett. **38** (1977) 956.

[4] C.J. Oram, J.M. Bailey, P.W. Schmor, C.A. Fry, R.F. Kiefl, J.B. Warren G.M. Marshall, and A. Olin, *Measurement of the Lamb Shift in Muonium.* Phys. Rev. Lett. **52** (1984) 910.

[5] A. Badertscher, S. Dhawan, P.O. Egan, V.W. Hughes, D.C. Lu, M.W. Ritter, K.A. Woodle, M. Gladisch, H. Orth, G. zu Putlitz, M. Eckhause, J. Kane, F.G. Mariam, and J. Reidy, *Formation of Muonium in the 2S State and Observation of the Lamb Shift Transition.* Phys. Rev. Lett. **52** (1984) 914.

[6] B. Ni, K.-P. Arnold, F. Chmely, V.W. Hughes, S.H. Kettell, Y. Kuang, J. Markey, B.E. Matthias, H. Orth, H.R. Schaefer, K. Woodle, M.D. Cooper, C.M. Hoffman, G.E. Hogan, R.E. Mischke, L.E. Piilonen, R.A. Williams, M. Eckhause, P. Guss, J. Kane, J. Reidy, and G. zu Putlitz, *Search for Spontaneous Conversion of Muonium to Antimuonium.* Phys. Rev. Lett. **59** (1987) 2716.

[7] T.M. Huber, G.A. Beer, T. Bowen, C.A. Fry, Z. Gelbart, P.G. Halverson, A.C. Janissen, K.R. Kendall, A.R. Kunselman, G.M. Marshall, G.R. Mason, A. Olin, and J.B. Warren, *Search for Mixing of* $(\mu^+ e^-)$ *and* $(\mu^- e^+)$ *with Fermi Coupling Strength.* Phys. Rev. Lett. **61** (1988) 2189.

[8] V.W. Hughes, D.W. McColm, K. Ziock, and R. Prepost *Formation of Muonium and Observation of its Larmor Precession.* Phys. Rev. **A5** (1960) 63.

[9] B.A. Barnett, C.Y. Chang, G.B. Yodh, J.B. Carroll, M. Eckhause, C.S. Hsieh, J.R. Kane, and C.B. Spence, *Muonium-formation measurement in low-pressure argon gas.* Phys. Rev. **A11** (1975) 39.

[10] S. Chu, A.P. Mills, Jr., A.G. Yodh, K. Nagamine, Y. Miyake, and T. Kuga, *Laser Excitation of the Muonium 1S-2S Transition.* Phys. Rev. Lett., **60** (1988) 101.

[11] P.R. Bolton, A. Badertscher, P.O. Egan, C.J. Gardner, M. Gladisch, V.W. Hughes, D.C. Lu, M. Ritter, P.A. Souder, J. Vetter, G. zu Putlitz, M. Eckhause, and J. Kane, *Observation of Muonium in Vacuum.* Phys. Rev. Lett. **47** (1981) 1441.

[12] C.J. Oram, C.A. Fry, J.B. Warren, R.F. Kiefl and J.H. Brewer, *Observation of the 2S state of muonium in a vacuum.* J. Phys. **B 14** (1981) L789.

[13] K.R. Kendall, Ph.D. thesis, University of Arizona, 1972 (unpublished).

[14] A.P. Mills, Jr., J. Imazato, S. Saitoh, A. Uedono, Y. Kawashima, and K. Nagamine, *Generation of Thermal Muonium in Vacuum.* Phys. Rev. Lett. **56** (1986) 1463.

[15] G.M. Marshall, J.B. Warren, D.M. Garner, G.S. Clark, J.H. Brewer, and D.G. Fleming, *Production of Thermal Muonium in the Vacuum between the Grains of Fine Silica Powders.* Phys. Rev. **A65** (1978) 351.

[16] *Cab-O-Sil Properties and Functions.* Technical report available from Cabot Corporation, 125 High Street, Boston, MA 02110, USA.

[17] B. Mandelbrot, *Fractals, Form, Chance, and Dimension,* Freeman, San Francisco, 1977.

[18] T.A. Witten, Jr. and L.M. Sander, *Diffusion-Limited Aggregation, a Kinetic Critical Phenomenon.* Phys. Rev. Lett. **47** (1981) 1400.

[19] R. Kiefl, J.B. Warren, G.M. Marshall, C.J. Oram, J.H. Brewer, D.J. Judd, and L.D. Spires, *Muonium and Positronium Production in Oxide Powders.* Hyperfine Interactions, **6** (1979) 185.

[20] G.M. Marshall, J.B. Warren, C.J. Oram, and R. F. Keifl, *Search for muonium-to-antimuonium conversion.* Phys. Rev. **D25** (1982) 1174.

[21] G.M. Marshall, Ph.D. thesis, University of British Columbia, 1981 (unpublished).

[22] B. O'Shaughnessy and I. Procaccia, *Diffusion on fractals.* Phys. Rev. **A32** (1985) 3073.

[23] G.A. Beer, G.M. Marshall, G.R. Mason, A. Olin, Z. Gelbart, K.R. Kendall, T. Bowen, P.G. Halverson, A.E. Pifer, C.A. Fry, J.B. Warren, and A.R. Kunselman, *Emission of Muonium into Vacuum from a Silica-Powder Layer.* Phys. Rev. Lett. **57** (1986) 671.

[24] C. Kittel and H. Kroemer, *Thermal Physics.* Freeman, San Francisco, 1980, p. 395.

[25] *CRC Handbook of Chemistry and Physics.* The chemical and Rubber Company, 60 th ed., Boca Raton, Florida, 1979.

[26] The Monte Carlo program MUBEAM was written for the MUBAR experiment by T. Bowen and P.G. Halverson of the University of Arizona with major modifications by A. Olin of TRIUMF. A listing is available from the Department of Physics, University of Victoria, VPN-89-1.

[27] V.L. Highland, Nucl. Inst. and Meth. **129** (1975) 497, and Nucl. Inst. and Meth. **161** (1979) 171.

[28] F. Mohling, *Statistical Mechanics.* Wiley, USA, 1982, problem I.6, page 43.

[29] C.A.M Mulder and J.G. van Lierop, *Preparation, Densification and Characterization of Autoclave Dried SiO_2 Gels* Aerogels, J. Fricke ed., Springer-Verlag, Berlin, 1985, page 68.

[30] G. Schuck and W. Dietrich, *Pore Size Distribution of Silica Systems* Aerogels, J. Fricke ed., Springer-Verlag, Berlin, 1985, page 148.

[31] K.A. Woodle, K.-P. Arnold, M. Gladisch, J. Hofmann, M. Janousch, K.P. Jungmann, H.-J. Mundinger, G. zu Putlitz, J. Rosenkranz, W. Schafer, G. Schiff, W. Schwarz, V.W. Hughes, and S.H. Kittell, *Measurement of*

the polarization of thermal muonium in vacuum. Z. Phys. **D9** (1988) 59-64.

Vita

Surname: Janissen **Given Names:** Anna Cornelia

Place of Birth: Calgary, Alberta **Date of Birth:** June 7, 1965

Universities Attended:

University of Calgary	1983 to 1984
University of Regina	1984 to 1984
University of Calgary	1984 to 1987
University of Victoria	1987 to 1989

Degrees Awarded:

B.Sc. Hon. University of Calgary, 1987

Honors and Awards:

Wescott Memorial Scholarship, TRIUMF (1988)

NSERC Postgraduate Scholarship (1987, 1988)

Presidents Research Award, University of Victoria (1987, 1988)

NSERC Undergraduate Research Award, University of Victoria (1986, 1987)

University of Calgary merit award (1985, 1986)

Viscount Bennett Scholarship, University of Calgary (1985)

Husky Oil Scholarship, University of Regina (1984)

Alexander Rutherford Scholarship, University of Calgary (1983)

Calgary Herald Centennial Bursary, University of Calgary (1983)

University of Calgary Matriculation Merit Award (1983)

Publication:

Search for Mixing of (μ^+e^-) and (μ^-e^+) with Fermi Coupling Strength.
T.M. Huber, G.A. Beer, T. Bowen, C.A. Fry, Z. Gelbart, P.G. Halverson, A.C. Janissen, K.R. Kendall, A.R. Kunselman, G.M. Marshall, G.R. Mason, A. Olin, and J.B. Warren, Phys. Rev. Lett. **61** (1988) 2189.

Partial Copyright License

I hereby grant the right to lend my thesis (the title of which is shown below) to users of the University of Victoria Library, and to make single copies only for such users, or in response to a request from the library of any other university or similar institution, on its behalf or for one of its users. I further agree that permission for extensive copying of this thesis for scholarly purposes may be granted by me or a member of the university designated by me. It is understood that copying or publication of this thesis for financial gain shall not be allowed without my written permission.

Title of Thesis:

MUONIUM PRODUCTION FROM FINE SILICA POWDER

Author: Anna Cornelia Janissen

March 15, 1989

ISBN 0-315-50169-3

Canada